R. & M. No. 1859
(2301, 3023, 3071, 3123, 3281)
A.R.C. Technical Report, 1938

AIR MINISTRY

AERONAUTICAL RESEARCH COMMITTEE
REPORTS AND MEMORANDA

General Investigation into the Characteristics of the C.30 Autogiro

By
P. A. Hufton, M.Sc., A. E. Woodward Nutt, B.A.,
F. J. Biog and J. A. Beavan, B.A.
With an Introduction by C. N. H. Lock, M.A.
and an Appendix by S/Ldr. H. P. Fraser

LONDON: HIS MAJESTY'S STATIONERY OFFICE
Price 10s. 0d. net

AERODYNAMIC SYMBOLS

GENERAL

m	Mass
t	Time
V	Resultant linear velocity
Ω	Resultant angular velocity
ρ	Density, σ relative density
ν	Kinematic coefficient of viscosity
R	Reynolds number, $R = Vl/\nu$ (where l is a suitable linear dimension)

Normal temperature and pressure for aeronautical work are 15° C and 760 mm.

For air under these conditions $\rho = 0{\cdot}002378$ slug/cu. ft.; $\nu = 1{\cdot}59 \times 10^{-4}$ sq. ft./sec.

The slug is taken to be 32·2 lb.-mass.

α	Angle of incidence
ϵ	Angle of downwash
S	Area
b	Span
c	Chord
A	Aspect ratio, $A = b^2/S$
L	Lift, with coefficient $C_L = L/\frac{1}{2}\rho V^2 S$
D	Drag, with coefficient $C_D = D/\frac{1}{2}\rho V^2 S$
γ	Gliding angle, $\tan\gamma = D/L$
L	Rolling moment, with coefficient $C_l = L/\frac{1}{2}\rho V^2 bS$
M	Pitching moment, with coefficient $C_m = M/\frac{1}{2}\rho V^2 cS$
N	Yawing moment, with coefficient $C_n = N/\frac{1}{2}\rho V^2 bS$

AIRSCREWS

n	Revolutions per second
D	Diameter
J	V/nD
P	Power
T	Thrust, with coefficient $k_T = T/\rho n^2 D^4$
Q	Torque, with coefficient $k_Q = Q/\rho n^2 D^5$
η	Efficiency, $\eta = TV/P = Jk_T/2\pi k_Q$

General Investigation into the Characteristics of the C.30 Autogiro

PART I. Performance and Aerodynamic Characteristics
PART II. General Blade Motion

By

P. A. HUFTON, A. E. WOODWARD NUTT and F. J. BIGG
of the R.A.E.
and
J. A. BEAVAN, of the N.P.L.

With an Introduction by C. N. H. LOCK
and an Appendix by S/Ldr. H. P. FRASER

Reports and Memoranda No. 1859
March, 1939

CONTENTS

PART II

General blade motion in gliding flight

INTRODUCTION

By

C. N. H. LOCK, M.A.

The present report on the performance of a gyroplane contains the first really satisfactory set of full scale data to be obtained in this country, and affords a valuable means of checking a body of theoretical investigation which has been growing up during the past twelve years. The greater part of this gyroplane theory can be transferred with little change to the case of the helicopter, on which full scale evidence is still almost completely lacking. In particular, the freedom of the blades to flap, which has played a considerable part in increasing the difficulty of gyroplane theory, seems likely to become an essential feature of all helicopters.

The first general account of the novel type of aircraft now known as the gyroplane appeared in this country in February, 1925; during the following three years a considerable amount of research on the subject was carried out at the Royal Aircraft Establishment and the National Physical Laboratory. This work is described in a series of reports [1, 2, 3, 4, 5], and summarised in a report dated April, 1928.[6] The research up to that time consisted mainly of theory and of wind tunnel experiments; there was little direct full scale evidence as to the true performance. The model data included observations of flapping and of unsteady motion as well as performance and showed reasonably good agreement with theory.

Since the date of the above report,[6] a series of improvements has converted the original Cierva Autogiro C.6 into the present C.30. The chief mechanical improvement has been the fitting of a gearing for starting the rotor by the engine; this has greatly reduced the time and distance required in taking off. Among aerodynamic improvements, the most fundamental is the control by tilting the rotor head, with which is associated the elimination of the fixed wing and ailerons and of the rudder. A slight advance has been made with regard to streamlining, but the parasitic drag of the fuselage is still undesirably high. A further aerodynamic improvement has been a reduction of the solidity to slightly less than a quarter of its original value (0·19, 4 blades, to 0·047, 3 blades); the original symmetrical section has changed to a cambered section and the blade angle measured from zero lift has increased from 1·75° to 5·5°.* With the large decrease of solidity there has been combined an undesirable increase in thickness ratio from 11·4 per cent. to 17·1 per cent., but the associated increase of blade density is probably advantageous.

* In actual flight this value is reduced as a result of blade twist.

For some years after 1928 there was little further research on gyroplanes in this country though considerable progress was made in America[7,8,9]. Eventually in 1934 a full scale C.30 autogiro was acquired for experimental research at the Royal Aircraft Establishment.

At about the same time an enquiry was instituted into an accident to a C.30 autogiro. The accident was attributed (originally on the advice of the inventor) to a loss of control in a high speed dive caused by differential twisting of the port and starboard blades. This enquiry led ultimately to a detailed theoretical investigation of blade twist and was followed by an investigation of blade bending.

At the time when the full scale experiments on the C.30 autogiro were first proposed, it was suggested that estimates of the probable top speed, lowest speed and rate of climb should be made independently by members of the staff of the National Physical Laboratory and the Royal Aircraft Establishment on the basis of existing theory. The two estimates were in fair agreement with each other and with the subsequent full scale observations, but they showed that uncertainty as to the parasitic drag of the fuselage would seriously affect the estimate of top speed performance, and to a less extent that of rate of climb.

Accordingly, wind tunnel measurements of drag were made on a model fuselage at the National Physical Laboratory, both in an atmospheric tunnel and in the Compressed Air Tunnel.

The twisting of the rotor blades is a fault in this particular aircraft which it is hoped to remedy in future designs by adopting a more stable section and by mass balancing the blades. The twisting has materially increased the difficulty of comparison between theory and experiment; the fact that it gave occasion for a research into the theory of twisting may perhaps be considered as some compensation.

The present report contains an account of nearly all the research on the C.30 autogiro up to the present time and its contents may be summarised as follows :—

Part I.—Full scale performance tests including :—direct measurement of maximum level speed, minimum level speed and maximum rate of climb; measurement of lift, drag, rotational speed and control setting for trim in glides at angles of incidence ranging from 70° to 3°. These results are compared with calculations of performance, based on the revised theory including the effect of twist, and on the parasitic drag of the fuselage deduced from wind tunnel experiments.

Part II.—Full scale measurements of blade motion by means of a ciné camera attached to the rotor hub. This determines the angular position of stations on the leading and trailing edges at various radii and so includes flapping, coning, motion in yaw, bending and twisting. All these measurements are compared with theory.

The most important features of the report will now be discussed in more detail.

General performance.

Maximum level speed at sea level	94 m.p.h.
Minimum level speed at sea level	32 m.p.h.
Maximum rate of climb	355 ft./min.
Service ceiling	6,600 ft.
Distance to take-off—no wind	450 ft.
Distance to 50 ft.—no wind	1,510 ft.
Distance from 50 ft. to touch—no wind	230 ft.
Distance from touch to rest—no wind	70 ft.
Minimum rate of descent	13 ft./sec.
Minimum angle of glide	11°
Steepest angle of controlled glide	45°

In comparing theoretical with observed performance in a glide, theoretical values of the rotor drag, based on assumed mean values of blade drag coefficient $C_D = 0{\cdot}012$ and $0{\cdot}014$, are added to the drag of the fuselage deduced from model tests, and compared with observed values of the total drag of the aircraft. The assumed values for the blade drag coefficient are higher than the values of profile drag corresponding to the mean lift coefficient of the section obtained in the Compressed Air Tunnel and the difference is to be attributed to the large variation of blade incidence, especially on the retreating blade, at small incidences of the aircraft. Thus the comparison really determines a value of mean C_D to fit the experiments and the conclusion is that this can be done with reasonable values of C_D.

At high forward speeds the observed drag of the rotor becomes greater and the lift smaller than the theoretical values for constant C_D of the blade section; this result is to be expected from the stalling of the central part of the retreating blade.

The drag deduced from the maximum flying speed agrees fairly well with that deduced from glides and is perhaps rather more reliable on account of the uncertainty of the drag of the idling propeller.

Steep descents.

Lowest gliding speed reached	22 m.p.h.
Rate of descent at lowest gliding speed	30 ft./sec.
Steepest angle of glide	68½°
Maximum lift coefficient (based on disc area)	1·10
Maximum resultant force coefficient (approx.)	1·4

The observations at very high incidences appear to have established the fact that the speed of vertical descent would be of the same order as that of a parachute of the same disc area. Although the highest incidence reached was 72° there is little chance of any appreciable change of normal force coefficient within the range 70° to 90°. This result seems to rule out the much slower rate of descent suggested by some earlier doubtful full scale experiments (R. & M. 1108, p. 2), and confirms a prediction made before the autogiro was known in this country.

Minimum speed in level flight.

	Measured.	*Predicted.*
Minimum level speed at 1,900 lb.	32 m.p.h.	36½ m.p.h.
Minimum level speed at 1,700 lb.	28 m.p.h.	31 m.p.h.
Minimum level speed at 1,560 lb.	23½ m.p.h.	27 m.p.h.

It appears on investigation that the minimum speed of steady flight is limited only by engine power and controllability; subject to control limitations the minimum speed would decrease indefinitely with increase of thrust, and the ultimate limit would only be reached when the thrust became equal to the weight of the aircraft. The full scale experiments also showed that the minimum flying speed varied considerably with the weight, the minimum speed falling by 8½ m.p.h. for a reduction of weight from 1,900 lb. to 1,560 lb. Theoretical calculations, while somewhat overestimating the minimum speed for given weight, give a slightly higher change (9½ m.p.h.) for the same change of weight.

It is considered that a sufficient explanation has been given of the demonstration flights in which the aircraft is raced by a running man; such stunts are at any rate far less dangerous than the flight of a normal aeroplane close to the stall since any instability is far less catastrophic.

General blade motion.—The observations made with the ciné camera on the hub represent perhaps the most interesting part of the investigation from the theoretical point of view. These observations determine the blade flapping, coning, twisting and bending, which are found to agree, almost without exception, with theoretical predictions, within the limits of experimental error.

General flying qualities.—The remarks by the pilot as to controllability are put clearly and briefly in an appendix to the report, and the main conclusion is that the addition of a rudder would be desirable for landing and low speed manœuvres. The addition of an elevator is desirable and indeed essential for safety in a high speed dive, unless the longitudinal instability can be cured by removing the tendency of the blades to twist.

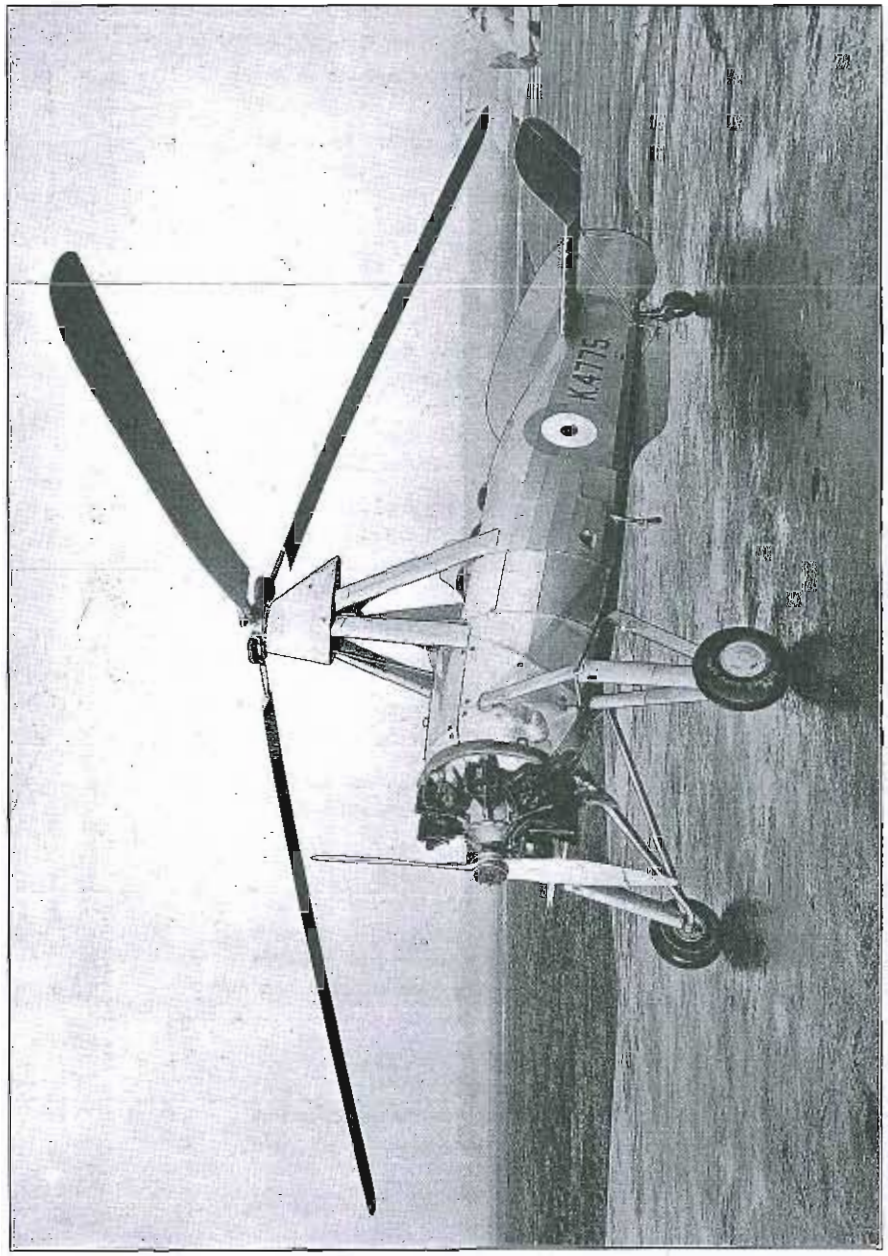

FIG. 1.—C.30 Autogiro.

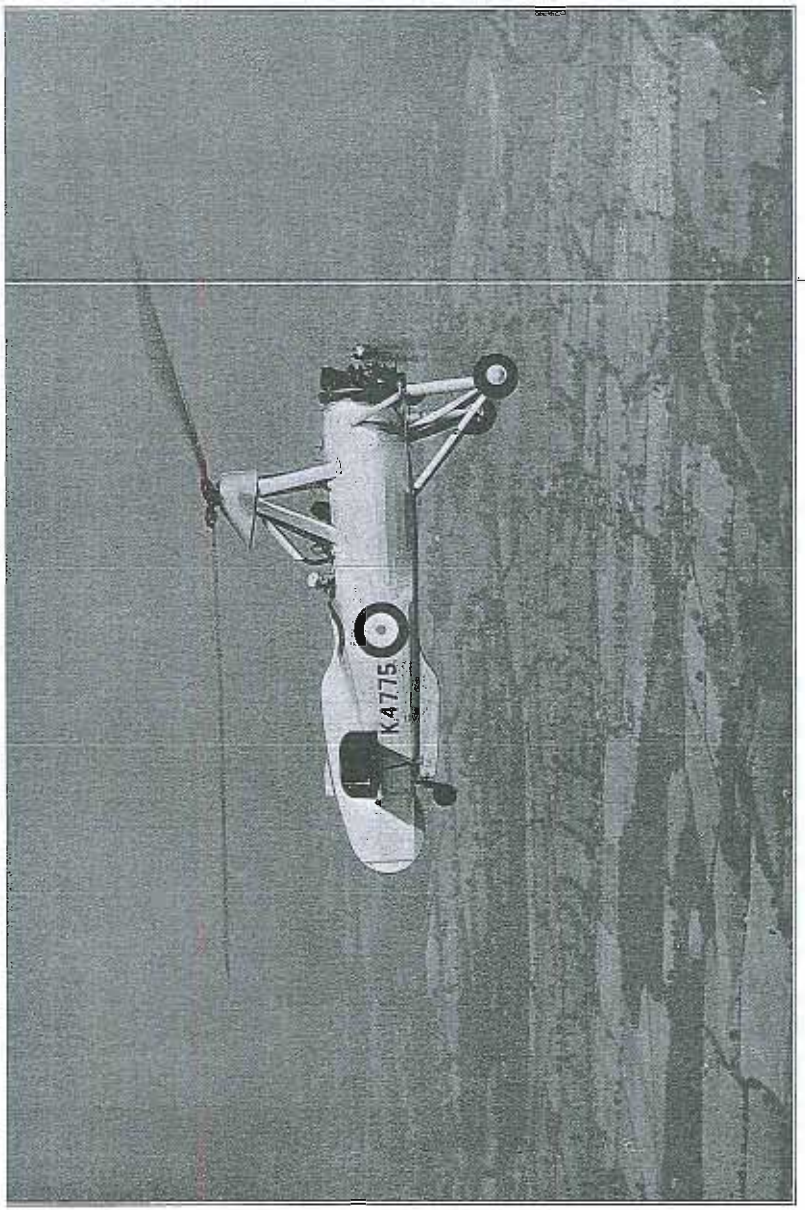

FIG. 2.—C. 30 Autogiro.

Conclusions.—The experiments do not suggest any very obvious method of improving the performance of the aircraft except by reducing the parasitic drag of the fuselage. It has been estimated that the reduction of solidity and increase of blade angle as compared with the C.6 autogiro has increased the L/D ratio of the rotor at top speed from 5·9 to 8·8, and it seems unlikely that much further improvement in the aerodynamic performance of the rotor can be obtained.

It has been shown by various authors that from a theoretical point of view there is a very close resemblance between the autogiro and the helicopter; so much so that in forward flight the equation of the latter can be derived from that of the former by a mere change of sign together with the suppression of the zero torque condition. This resemblance extends to all details such as flapping, twisting and bending of the blades. These considerations will very considerably increase the value of the present work to those who believe in the future of the helicopter and consider the gyroplane principally as a step in its development.

Certain gaps in existing theoretical knowledge are brought out by the present investigation. There is still little information as to the effect of the stalling of the blade sections in limiting the maximum blade angle at which autorotation is possible and safe. Some attempts at calculation made at the time of the model tests (R. & M. 1154[5]) did not give good agreement with experiment.

The outstanding problem of both gyroplane and helicopter is that of stability. This is likely to prove even more difficult than the work that has been done up to the present, but a start is now being made by several investigators, and it is to be hoped that success will ultimately be reached.

PART I

Performance and aerodynamic characteristics

1. *Description of aircraft.*—The C.30 type autogiro is an open two-seater with a 140 H.P. Civet I engine. Except for minor details the autogiro tested was similar to the standard "Rota" type in the R.A.F. Photographs of the autogiro are given in Figs. 1 and 2, and the principal dimensions and particulars in Table 10 (at the end of the report).

The rotor is 3 bladed and of 37 ft. diameter. The section of the blades closely resembles Göttingen 606, and the blade chord is 11 in. The solidity (defined as $bc/\pi R$, where b is the number of blades, c the blade chord and R the rotor radius) is therefore 0·0472. A plan and section of a blade are given in Fig. 3.

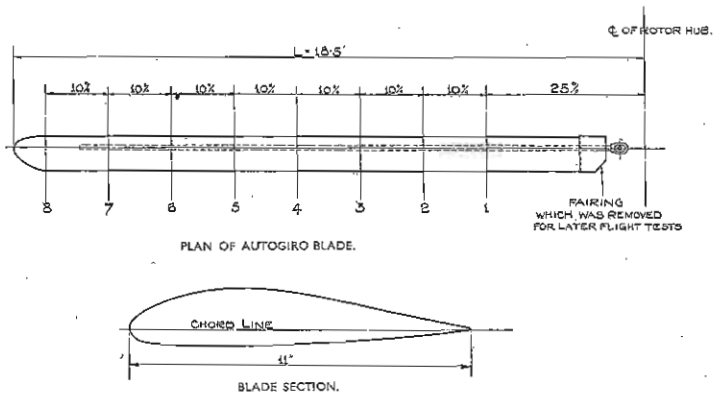

FIG. 3.—Autogiro Blade.

The fin and tail surfaces are fixed, control being effected by tilting the rotor shaft laterally and longitudinally. This is done by an inverted control column pivoted at the rotor head and tilting the head through link mechanisms. A forward or backward movement of the control tilts the rotor head, and hence the line of action of the resultant force, in the opposite direction, thus causing the nose of the autogiro to fall or to rise. A lateral movement of the control tilts the head in the opposite direction laterally, causing bank and then sideslip, which in turn generates yaw in the required direction. Diagrams showing the linkages are given in Fig. 4. Longitudinal and lateral trim is obtained by adjusting the tension of springs, which constrain the control column in the appropriate planes. Directional control on the ground is provided by a swivelling tail wheel coupled to a rudder bar.

Initial rotation of the blades on the ground is obtained by driving them from the engine through a friction clutch, bevel gear and dog clutch. The normal rate of rotation reached on the ground is about 185 r.p.m., the r.p.m. during normal flight

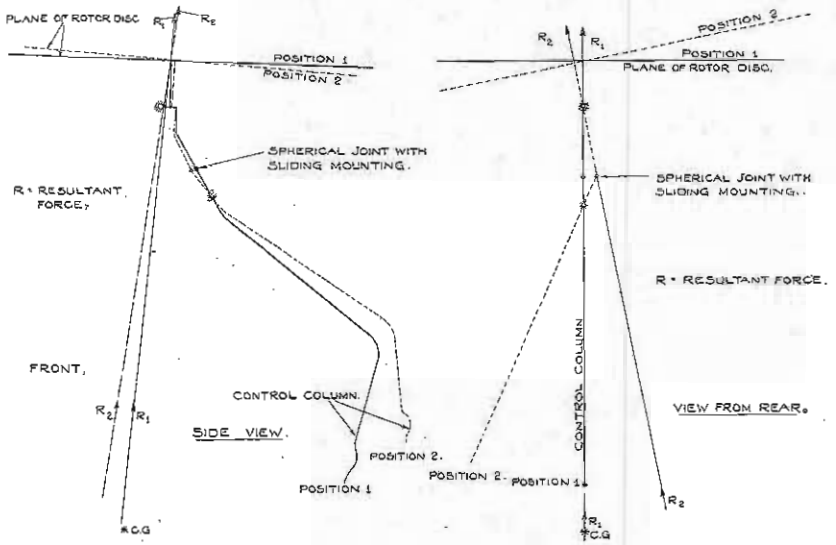

FIG. 4.—Control linkages and resultant forces on rotor disc.

being 200–240. To take off, the clutch is slipped and the autogiro allowed to run along the ground until an air speed sufficient for autorotation of the blades at flight speed is attained (for details *see* Appendix I).

The fixed tail plane has upturned tips to provide an additional yawing moment for turning, and has positive camber on the right hand side and negative on the left to counteract to some extent the engine torque, the engine rotating anti-clockwise. Small trimmer tabs, adjustable on the ground only, are attached to the trailing edges of the tail plane for the same purpose.

The total loaded weight of the autogiro as flown in the tests at full load was approximately 1,900 lb. The position of the centre of gravity was 6 in. aft of the junction of the front pylon struts and the top longeron, measured parallel to the longeron. Tests were also made at a total weight of 1,700 lb., and measurements of the minimum speed at the least possible load of 1,560 lb. Weight analyses in these three conditions are given in Table 1.

TABLE 1

Weight analyses

	Full load.	Reduced load.	Minimum load.
Tare weight	1,261 lb.	1,261 lb.	1,261 lb.
Pilot and parachute	200 lb.	200 lb.	180 lb.*
Observer and parachute	200 lb.	—	—
Fuel	177 lb.	138 lb.	38 lb.
Oil	30 lb.	30 lb.	30 lb.
Special instruments, etc.	29 lb.	67 lb.	50 lb.
Total loaded weight ..	1,897 lb.	1,696 lb.	1,559 lb.

* Pilot had no parachute.

2. *Particulars of tests made.*—In the first place handling tests were made by a number of pilots to investigate the features of the direct control, and to compare the behaviour of the autogiro with that of an aeroplane. They were followed by performance tests at full load. These comprised measurement of the maximum and minimum speeds in level flight at various heights, and determination of the maximum rate of climb curve for full throttle climbs to the service ceiling, the best climbing speeds having previously been determined from partial climbs at two heights. The level speeds were measured using a suspended air log, the maximum speed at ground level being checked by a number of runs over a speed course.

Similar performance measurements were made at the reduced load of 1,700 lb. In addition, as a minor repair had been made to the engine, and the rotor blades had been changed since the determination of the full load performance, it was considered advisable to check the latter. Accordingly measurements were made of the maximum and minimum speeds at full load in level flight near the ground. All results have been reduced on the $p\sigma t$ basis.

A series of measurements of the minimum speed of the autogiro at the least possible load was made, by timing it along a speed course on the aerodrome at various heights. For reasons of safety, they were not made at full throttle, but the performance at full throttle may be estimated from the results. In certain cases ciné-photographs were taken of the autogiro flying over the special speed course, and from these films the speed, height and attitude throughout the runs were deduced.

Take-off and landing distances at both full load and reduced load were measured using a ciné camera.

In addition to the performance measurements, glides with the engine throttled right back were made over a wide range of speeds, and the air speed, rate of descent,

attitude, rotor r.p.m., and control position measured,* and the principal aerodynamic characteristics of the autogiro deduced from the results. The speed was measured by a low reading suspended air log, modified so that it lay along the flight path for steep angles of descent. The effect of the proximity of the aircraft on the speed as measured by the air log has been calculated and found to be negligible throughout. The fore and aft position of the hanging control was given by a scale and pointer at the rotor head, read in a mirror in the cockpit, and so arranged that the readings were unaffected by lateral movements of the control. The other quantities were measured as on an aeroplane.

3. *Preliminary calibrations, and particulars of blades.*—Before starting the tests, the rotor blades were removed and the incidence of each blade checked at a number of stations along its span. The results are given in Table 2. The method of finding the mean blade incidence is that adopted by Messrs. Cierva, and consists of multiplying the incidence at each station by a factor depending on the distance of the station from the blade root, before averaging the results.

TABLE 2

Blade incidence for 1st set

Position. †	Blade incidence.		
	Blade 431c.	Blade 441c.	Blade 417c.
1	2° 52′	2° 58′	2° 49′
2	2° 52′	2° 59′	3° 12′
3	2° 59′	2° 59′	3° 5′
4	3° 2′	2° 47′	3° 0′
5	3° 5′	2° 37′	2° 57′
6	3° 1′	2° 43′	2° 42′
7	3° 3·5′	2° 45′	2° 34′
8	2° 42′	2° 30′	2° 1′
Mean ..	2° 56′	2° 43′	2° 38′

† See Fig. 3 for positions along blade.

Mean blade incidence =

$$(\beta_1 + 1{\cdot}5\beta_2 + 2\beta_3 + 2{\cdot}5\beta_4 + 3\beta_5 + 4\beta_6 + 5\beta_7 + 6\beta_8)/25,$$

where β_1 = incidence at position 1, etc.

* Some of these quantities were measured in the course of the performance tests in addition.

After completion of part of the performance tests, the blades had to be removed and sent away for a modification which had to be made to all C.30 autogiro blades. Before despatch, the incidences were checked and found to be substantially the same as before. A second set of blades was received and calibrated, but on the first flight after fitting them two blades failed by splitting at the trailing edges. A third set was received some time later, the performance tests were finished and the gliding tests all made with these blades. The incidence measurements for the blades are given in Table 3.

TABLE 3

Blade incidence for 3rd set

Position.	Blade incidence.		
	Blade 539/B.	Blade 549/B.	Blade 544/B.
1	2° 51′	2° 34′	2° 55′
2	2° 54′	2° 30′	2° 53′
3	2° 49′	2° 32′	2° 48′
4	2° 41′	2° 30′	2° 56′
5	2° 41′	2° 29′	2° 46′
6	2° 30′	2° 21′	2° 57′
7	2° 23′	2° 24′	2° 48′
8	2° 17′	2° 24′	2° 20′
Mean ..	2° 32′	2° 26′	2° 44′

It will be seen that there are small differences between the first and third sets of blades, and in addition it was found necessary with the third set to remove some fairings near the roots, thus slightly reducing the total area (Fig. 3). The effect of these differences is just detectable in some of the curves of blade characteristics and will be referred to later, but a careful check revealed no measurable effect on the performance or aerodynamic characteristics of the complete aircraft.

The angular movement of the rotor head was also calibrated with respect to the movement of the hanging control column. The full angular movement of the control column longitudinally gave an angular movement of 10° to the rotor head, and the full lateral movement of the control gave a movement of 9° to the head. These movements were unaffected by the position of the lateral or longitudinal trimming controls.

4. *General flying qualities.*—A detailed pilot's report of the flying qualities of this autogiro is given in Appendix I. Briefly it may be said that under normal flying conditions, control with the hanging control column is straightforward and much simpler than that of an aeroplane. The control is heavy compared with that of a normal aeroplane, and there is an appreciable lag in the fore and aft control. Laterally, the autogiro rolls immediately the control is applied, but there is a definite time lag before the sideslip which follows has caused sufficient yaw to turn the aircraft.

The lack of a rudder is considered a serious drawback, particularly for correcting drift when landing and for directional control near the ground. (*See* Appendix I.) It has however been suggested that fitting a conventional rudder may cause some lateral instability.

In dives at speeds greater than about 115 m.p.h., the aircraft becomes nose heavy, and the force required on the control column increases slightly with speed. In recovery from a dive, the response of the autogiro to control movement is very slow. In view of this the maximum speed in the gliding tests was restricted to 110 m.p.h.

In glides at low speeds, control is maintained down to an air speed of about 22 m.p.h. When gliding at about this speed, if the control column is pulled back further, the aircraft yaws to the right and the nose drops. The lateral control is quite ineffective to prevent this. If the control column is pulled back when flying at low speeds with engine on, the autogiro assumes a very steep attitude, until eventually fore and aft control is lost, and the nose continues to rise (unless the throttle is closed) until the lateral control also breaks down and the aircraft yaws and falls away rapidly to the right.

The autogiro is unstable, but not violently so, both longitudinally and laterally. The lateral force on the control column varies with speed, and if the lateral bias is adjusted so that there is no lateral force on the column for intermediate speeds, the aircraft will tend to yaw to the left at low speeds and to the right at high speeds.

Any lack of balance between the blades causes vibration of the control column. On one occasion, small splits developed in the trailing edges of two blades during flight, causing the control column to vibrate through an amplitude of about 12 in. at high and 6 in. at low speeds. Thus the consequences of any accident to the lifting surfaces are magnified, and this must be considered a serious drawback to the hanging control column type of control. (*See* Appendix I, §11.9.)

It should be noted that both above and in Appendix I, attention has been concentrated on the special features possessed by the C.30 type autogiro by virtue of the direct control. The inherent features of the autogiro as compared with an aeroplane, *i.e.*, the ability to fly at low forward speeds and to land in confined spaces, are well known and have not been especially emphasised.

5. *Results.* 5.1. *Performance tests at full load.*—The maximum and minimum speeds in level flight and the corresponding engine r.p.m. are plotted against height in Fig. 5. It will be seen that the maximum speed at ground level is 94 m.p.h. at 2,250 r.p.m., and the minimum speed (which was found to occur at full throttle) is 32 m.p.h.* at 2,100 r.p.m. In Fig. 6 the rate of climb, time to height, and A.S.I. on climb curves are plotted. The maximum rate of climb is approximately 355 ft./min., and the service ceiling of approximately 6,600 ft. is reached in 33 minutes. The results have been reduced to standard conditions on the $p^{\frac{1}{2}}\sigma^{\frac{3}{2}}$ basis.

During the performance tests some measurements were made of rotor r.p.m., attitude of aircraft, control position, etc., from which various characteristic curves have been deduced. These will be considered later when discussing the results of the gliding tests.

5.2. *Performance tests at reduced load.*—Fig. 7 shows, plotted against height, the maximum and minimum speeds in level flight at full load (1,900 lb.), repeated from Fig. 5, and for the reduced load of 1,700 lb. In addition some check measurements of the maximum and minimum level speeds at full load are plotted. Fig. 8 gives time to height, and rate of climb curves for climbs to the service ceiling at both full load and reduced load. The A.S.I. for the best rate of climb was found to be the same for both loads. If allowances for the change of weight are made in accordance with R. & M. 984[10], the performances at the two loads are brought into good agreement.

It appears from Fig. 7 that the change in rotor blades and the overhaul of the engine have had no measurable effect on the performance and the measured performance at reduced load can be compared directly with that measured previously at full load. The main results are :—

	1,900 lb.	1,700 lb.
Maximum level speed (S.L.)	94 m.p.h.	97 m.p.h.
Minimum level speed (S.L.)	32 m.p.h.	28 m.p.h.
Maximum rate of climb (S.L.)	355 ft./min.	540 ft./min.
Ceiling (service)	6,600 ft.	9,400 ft.

5.3. *Minimum speed at least possible load.*—The reduction in minimum speed obtained by reducing the load from 1,900 lb. to 1,700 lb. was not sufficient to explain the extremely low speed obtained in demonstrations of the C.30 autogiro. Further tests were therefore made with as light a load as possible, to establish the minimum safe speed of flight near the ground. For these tests the autogiro was stripped of all unnecessary instruments and flown with five gallons of petrol only. In this condition the total weight was approximately 1,560 lb.

* For reasons of safety the lowest height at which the minimum level speed was measured was about 500 ft., and the speed at ground level was obtained by extrapolating the speed/height curve.

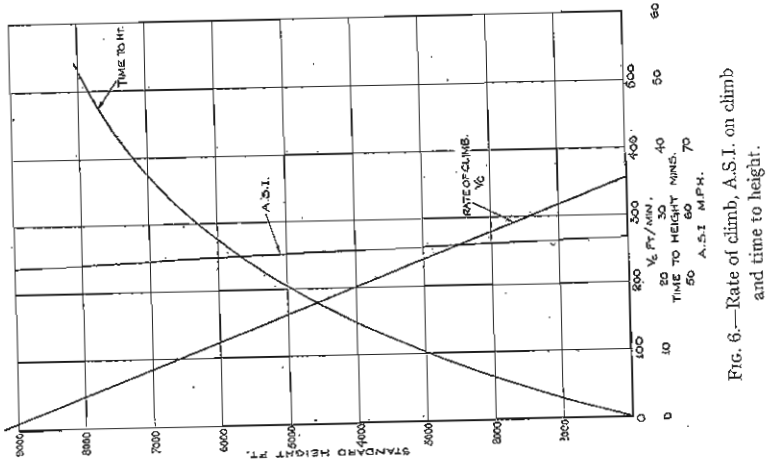

FIG. 6.—Rate of climb, A.S.I. on climb and time to height.

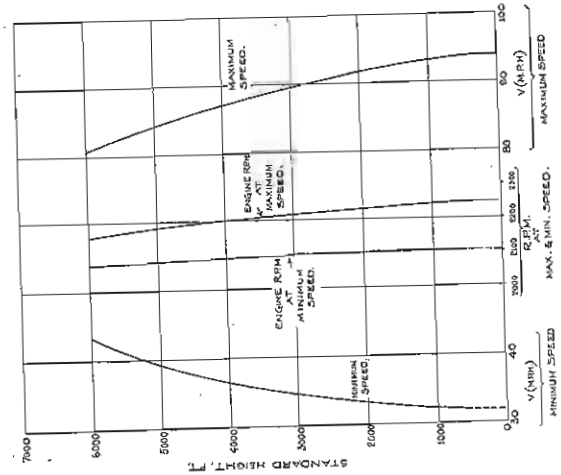

FIG. 5.—Maximum and minimum level speeds and corresponding engine r.p.m.

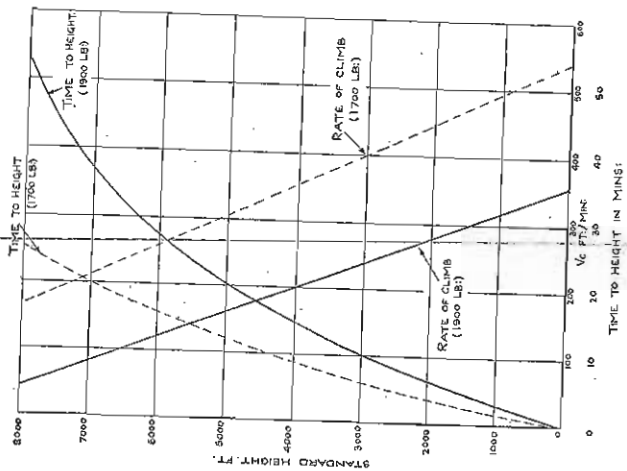

FIG. 8.—Rate of climb and time to height curves for loads of 1,900 lb. and 1,700 lb.

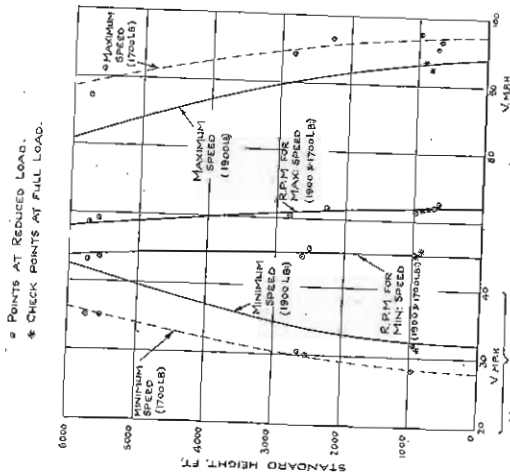

FIG. 7.—Maximum and minimum level speeds and corresponding engine r.p.m. for full load and reduced load.

Some of the flights at this weight were made by a pilot from the Cierva Autogiro Company. No distinction can be made between his runs, and those made by the Royal Aircraft Establishment pilot. Fig. 9 gives the results of the measurement of the ciné films of some of the flights.

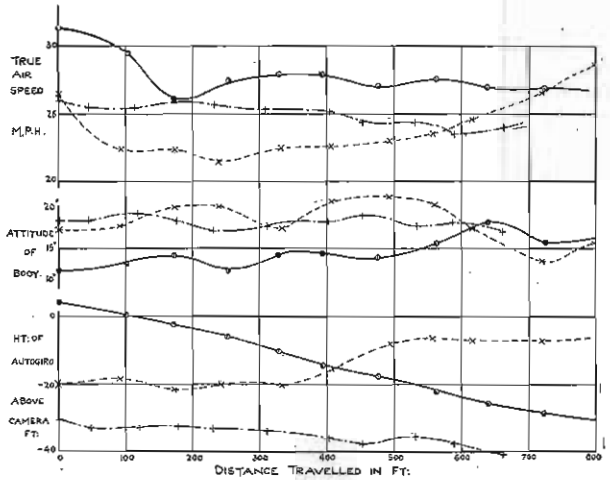

FIG. 9.—Speed, attitude and height on slow speed flights at least possible load.

It appears from the above that the airspeed can be reduced to about 22½ m.p.h. without any considerable loss in height (throttle setting unknown). For the complete run of 930 ft. however, the lowest mean speed is about 25 m.p.h. The rotor speed was measured from the films and found to be 182 r.p.m.

Some further runs over the speed course were not photographed and the mean values of the speed, engine revolutions, etc., for these runs were as follows :—

TABLE 4

True air speed.	Engine revolutions.	Mean height, ft.	Notes.
28·0 m.p.h.	1,990	5	3 runs, not full throttle.
27·3 m.p.h.	1,995	10	5 runs, not full throttle.
Minimum level speed	2,135	250	1 run, full throttle.

From the above figures, the average minimum level speed at 1,995 r.p.m. is 27½ m.p.h. Full throttle engine revolutions are however 2,135. Using these figures, the data for the engine and airscrew and the results of the glide tests, 23½ m.p.h. is estimated as the minimum level speed at full throttle. There is no evidence of any ground effect on minimum speed.

It is considered that this reduction of minimum level speed explains the slow flying demonstrations of the C.30 autogiro.

5.4. *Take-off and landing tests.*—Full notes on the take-off and landing of the autogiro are given in Appendix I, to which reference should be made.

5.41. *Take-off.*—A series of take-offs were made and photographed at full load (1,900 lb.) and reduced load (1,700 lb.). Table 5 below gives the data corrected to a zero wind speed.

TABLE 5

R.P.M. at declutch.	Velocity at take-off, m.p.h.	Velocity at 50 ft., m.p.h.	Distance to take-off, ft.	Distance from take-off to 50 ft., in ft.	Total distance, ft.
(a) 1,900 *lb.*					
210	39½	44	432	975	1,407
207	46½	45½	402	1,070	1,472
206	40	43	352	1,010	1,362
203	45½	42½	455	825	1,280
200	36½	54	463	978	1,441
195	37½	42½	478	1,202	1,680
195	38	50½	458	1,020	1,478
195	39½	55	463	1,196	1,659
195	38	60½	475	1,103	1,578
190	38	56½	465	1,062	1,527
185	38	50	471	1,270	1,741
		Average ..	443	1,065	1,510
(b) 1,700 *lb.*					
210	40½	43	290	604	894
208	37½	47	269	790	1,059
200	39½	40½	320	643	963
200	37	37½	270	588	858
200	37	36½	325	532	857
190	43	34	323	390	713
190	36½	36	327	508	835
180	39	38	340	543	883
170	39	40½	270	490	760
170	37½	37½	322	434	756
		Average ..	305	550	855

The following points regarding these figures are of interest :—

(a) The distance required for take-off does not bear any noticeable relation to the speed at take-off, nor does the reduction of rotor speed at the start of the run from 210 r.p.m. to 170 r.p.m. make any consistent difference to the take-off distance.

(b) With full load (1,900 lb.) the average distance required to take-off is 445 ft., and to reach 50 ft. from rest 1,510 ft. With reduced load (1,700 lb.) the average take-off distance is 305 ft., and the distance to reach 50 ft. from rest is 855 ft.

5.42. *Landing.*—Table 6 gives the results of landings made at two loadings, by two different pilots. They have all been corrected to zero wind speed.

There seems to be no relation between the velocity on the glide and the velocity at touch, the velocity at touch evidently depending to a large extent on how far and how quickly the stick is pulled back.

Similarly, no definite conclusion can be drawn from the fact that the average velocity at touch is lower for the lightly loaded autogiro than when it is heavily loaded, for the tests at light load were made by a pilot with greater flying experience on autogiros. It seems likely that the piloting was entirely responsible for the difference in touch speeds, and hence for the difference in landing run.

TABLE 6

Velocity at 50 ft., m.p.h.	Velocity at touch, m.p.h.	50 ft. high to touch, ft.	Touch to rest, ft.	Total distance, ft.
(a) *Full load* (1,900 *lb.*)				
39	23½	256	177	433
43½	24	254	166	420
42	19	318	96	414
39½	21	271	100	371
40	20½	284	106	390
49	25½	326	130	456
56½	25½	316	140	456
	Average ..	290	130	420
(b) *Reduced load* (1,700 *lb.*)				
39½	17½	331	88	419
34	10	264	39	303
39½	13½	327	60	387
27	13	232	57	289
41	13½	230	96	326
39	13	380	55	435
41	14½	390	80	470
38½	15	397	64	461
	Average ..	320	68	388

It is concluded that the average distance from 50 ft. to touch is about 300 ft., and the distance from touch to rest about 70 ft., for a pilot with moderate experience of an autogiro.

5.5. *Aerodynamic tests.*—The principal results of the gliding tests are given in Table 11 at the end of the report. Curves of lift, drag and total force coefficients (C_L, C_D and C_R), based on the total disc area, are plotted against the disc incidence i in Fig. 10. The disc incidence may be defined as the angle between the flight path and a perpendicular to the rotor axis lying in the plane of symmetry of the aircraft.

It will be seen from Fig. 10 that the maximum lift coefficient C_L is 1·10, and occurs at a disc incidence of about 31°. The total force coefficient becomes sensibly constant for incidences greater than about 37°, its value being about 1·36. This result is similar to that obtained by Wheatley[7] with a P.C.A.—2 autogiro in the U.S.A. The highest incidence reached was 72°.*

The attitude $(i - \gamma)$, gliding angle γ, and inclination of rotor axis to fuselage χ are plotted against C_L in Fig. 11. The top curve in this figure shows that the total change in the attitude of the aircraft over the range of incidence covered is approximately 14°, and that for steep descents the rotor disc is at a small positive angle to the horizontal.

From the curve of γ against C_L it will be seen that the minimum gliding angle is 11°, and occurs at a C_L of approximately 0·20. The steepest gliding angle reached in the tests was approximately 68° to the horizontal.* Glides at angles of this order are only possible by vigorous and skilful use of the controls (*see* Appendix), and the aircraft pitches and rolls considerably and is quite uncontrollable directionally. The steepest angle for steady glides is of the order of 45°. (*See* Appendix I, §§ 11.4 (*c*) and (*d*).)

The bottom curve in Fig. 11 shows that χ is sensibly constant over the range of speeds covered by the tests, which implies that the position of the control column is approximately the same for all speeds. In the very steep descents at low forward speeds the control column had to be moved fore and aft frequently to the full extent of its travel, so that the values for χ are relatively rough means of a widely varying quantity. At the other end of the speed range, there is some evidence that at speeds higher than those covered by the tests, the position of the

* These values are mean readings during a glide of about 2½ minutes' duration. The gliding angle γ was obtained from measurements of the total height loss and total distance travelled along the flight path during the measured time interval. The attitude was obtained by taking a mean of the series of readings of a visual inclinometer during the glide. Owing to the pitching of the aircraft, the inclinometer bubble was at times off the scale. For these unsteady glides, therefore, the values quoted for γ are true means of widely varying angles, and the values of $(i - \gamma)$, and hence i, are approximate means.

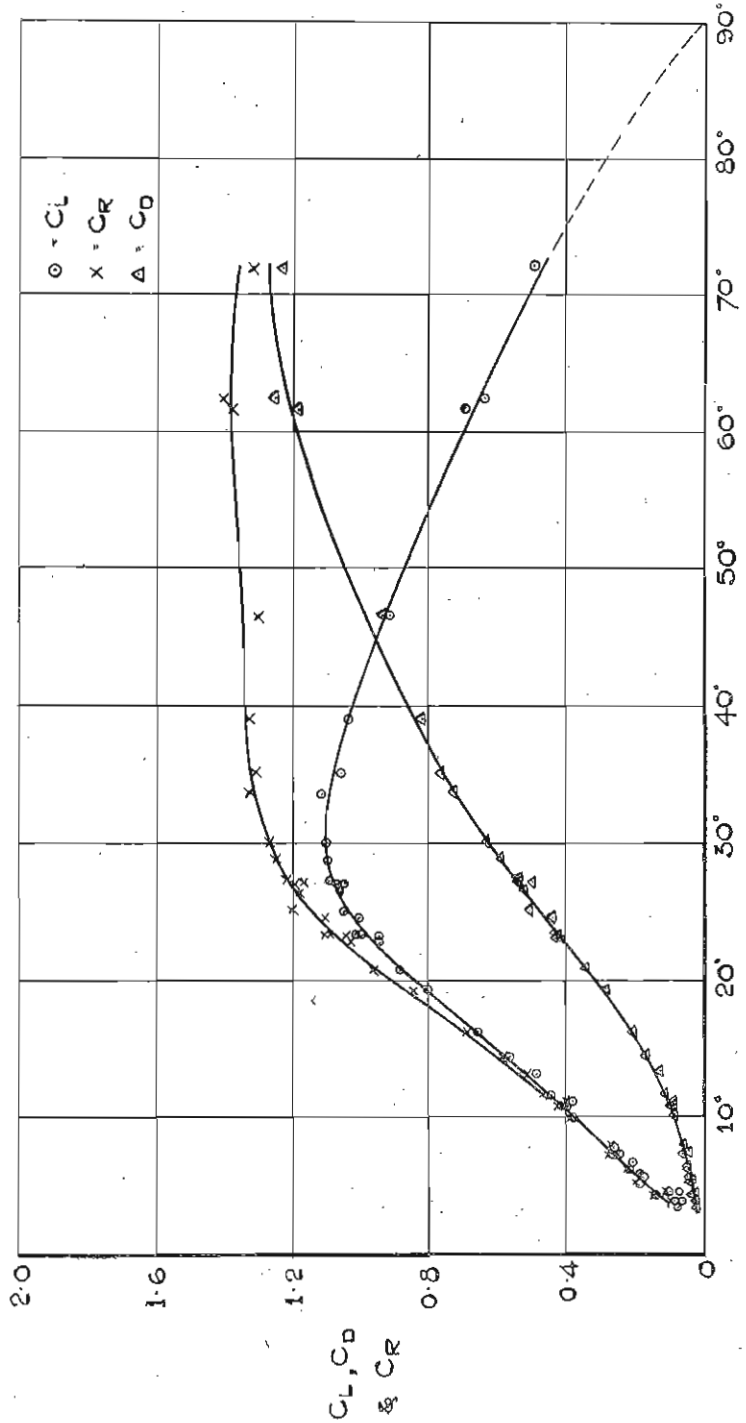

Fig. 10.—Lift, drag and total force curves.

control column to trim is further back, giving an increase of χ with speed. Over the normal flying range, however, the control column position may be taken as constant. Change of speed or attitude is effected by moving the control in the appropriate direction, but the control has to be centralised after the change has occurred. In §8 below may be found a discussion of such changes of χ as do occur.

The rate of descent — $v_0\sqrt{\sigma}$ and the r.p.m. of the rotor ($N\sqrt{\sigma}$) are plotted against indicated air speed (V_i) in Fig. 12. The minimum rate of descent will be seen to be 13 ft./sec. and the rate of descent in the steepest glides about 30 ft./sec. A line representing the condition $-v_0\sqrt{\sigma} = V_i$ is plotted on this figure and the intersection of this line and the experimental curve suggests that if vertical descent were possible, the rate of descent would be about 32 ft./sec. Very little change in the air speed occurs for wide variations in rate of descent at the low speed end. The second curve in Fig. 12 shows that the rotor r.p.m. vary roughly between 200 and 230 in flight over the speed range covered by the tests.

In Fig. 13, C_L and C_D have been plotted against the tip speed ratio $\mu = V \cos i/R\Omega$, where Ω is the angular velocity of the rotor and R its radius[4]. In Figs. 14 and 15, curves of disc incidence and speed against μ, obtained from the glides, are compared with results obtained during full throttle performance tests with two sets of blades. It will be seen that the three sets of results are in good general agreement, but that in the V_i/μ curve there is a small but definite displacement between the points obtained with the two sets of blades, particularly at the high speed end. This displacement is in a direction consistent with the small difference in mean incidence between the two sets of blades. The effect on performance was not measurable. There is a displacement of the same order between the results obtained in gliding flight and at full throttle with the same set of blades.

6. *Calculation of performance.* 6.1. *Comparison with performance tests and glides.* —Previous estimates of the performance of the C.30 autogiro had agreed in giving a higher maximum level speed and higher rate of climb than those measured in the performance tests.

Several causes for the discrepancy in performance can be advanced. No allowance was made for tip losses, nor for the change of blade incidence due to twist. Furthermore, the fuselage drag was based on an estimate only and, in order to determine how far the discrepancy was due to fuselage drag errors, a one-eighth scale model of the aircraft fuselage has since been tested at the National Physical Laboratory. This model was complete save for the airscrew and rotor blades (Fig. 16).

The details of the experimental method, a discussion of the scale effect on drag, and a comparison between the results of drag measurements made in a 7 ft. tunnel and in the Compressed Air Tunnel are contained in Appendix II.

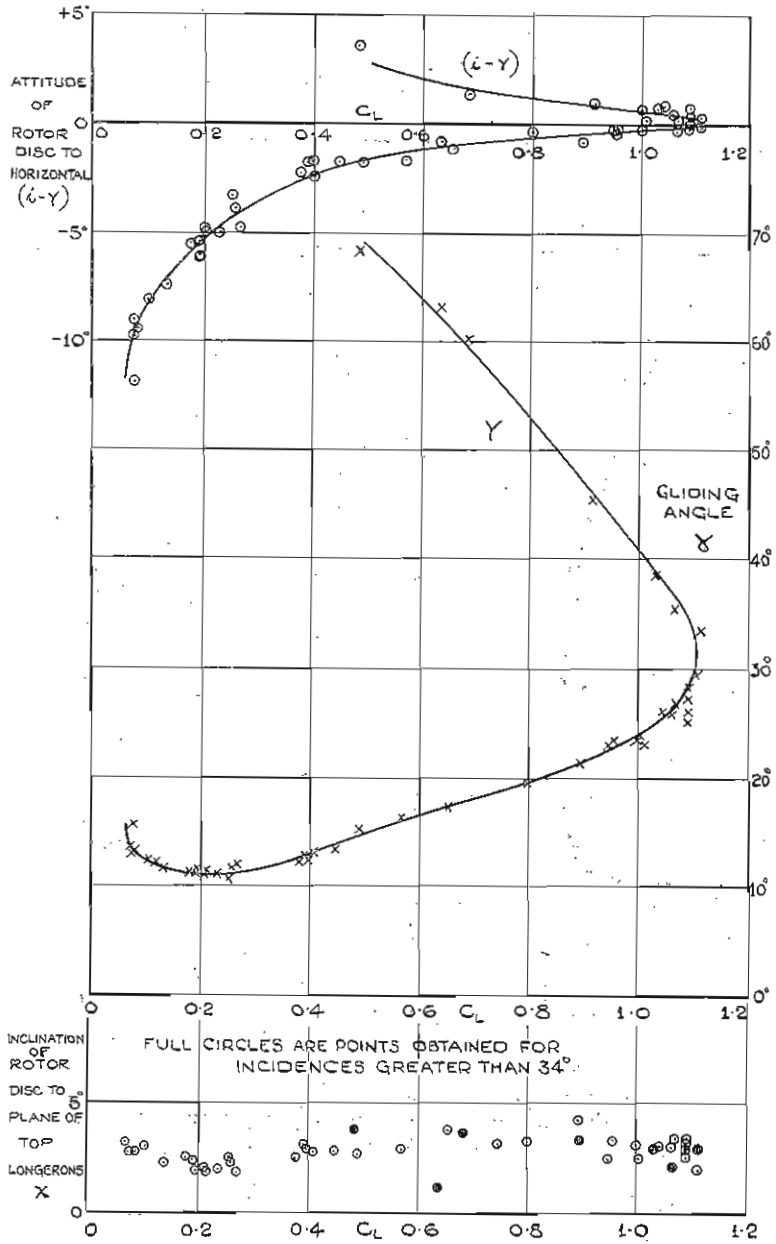

FIG. 11.—Attitude, gliding angle and trimming curves.

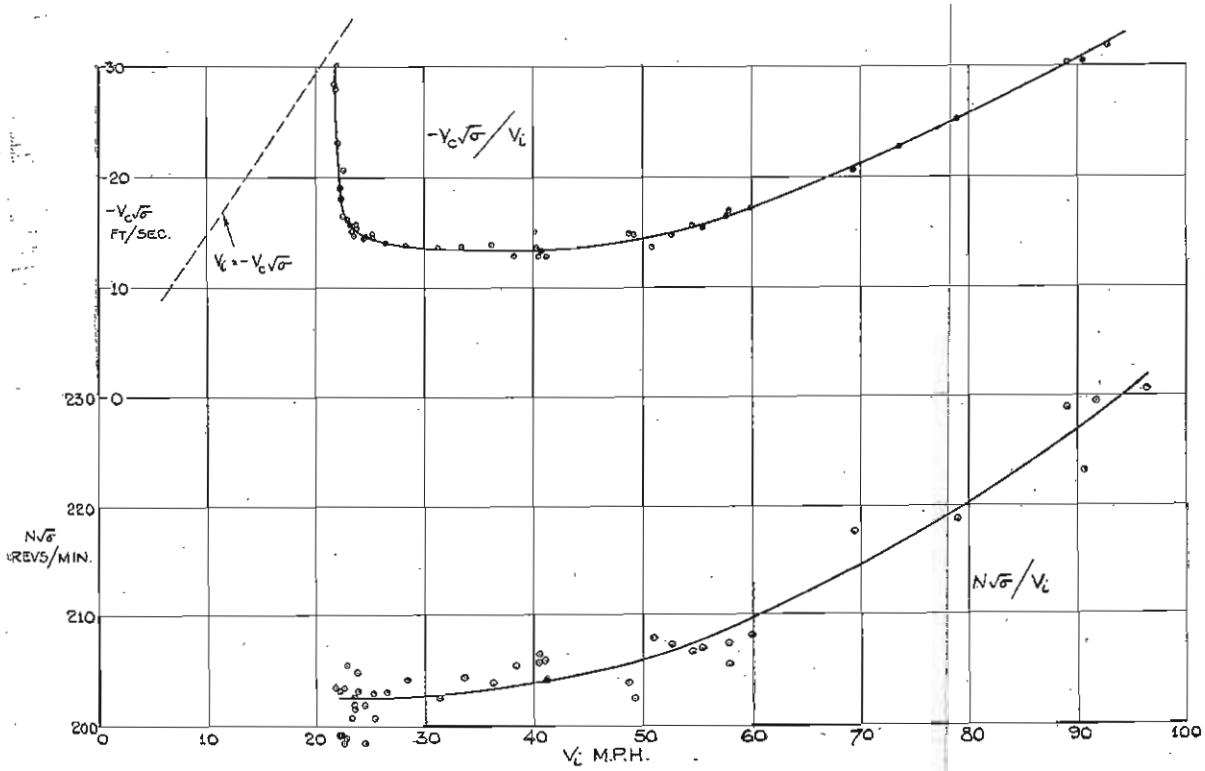

FIG. 12.—Rate of climb and rotor speed.

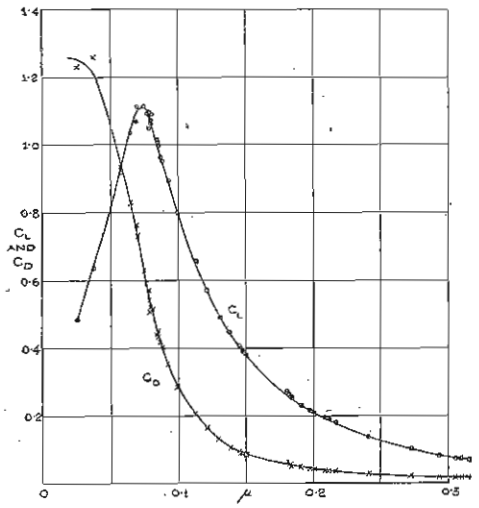

FIG. 13.—Lift and drag coefficients/tip speed ratio.

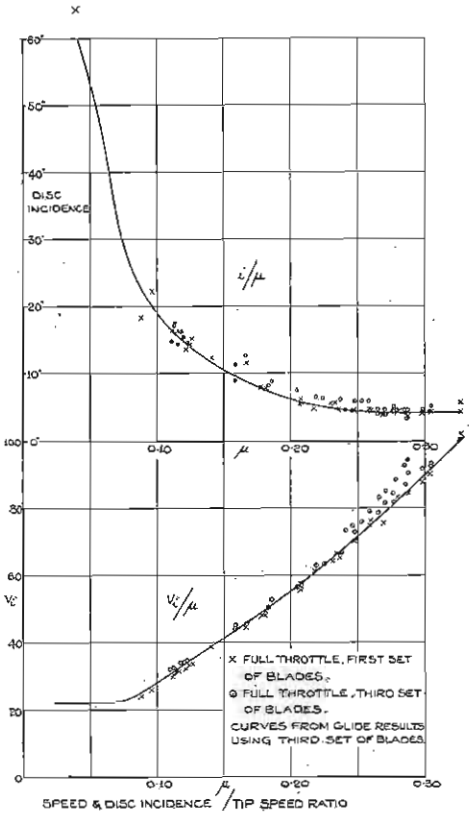

FIGS. 14 and 15.—Comparison of glide and full throttle results with two sets of blades.

An approximate figure of 90 lb. at 100 ft./sec. was obtained for the parasitic drag of the whole aircraft fuselage at zero incidence, the contributions of the various parts being as shown in the Appendix.

The lift and drag variations with incidence are plotted in Fig. 40 (Appendix II) for both the cases, tail plane present and removed. It may be seen that except when the aircraft is gliding steeply the parasitic drag, tail plane off, is nearly constant for varying incidence, and even when this latter reaches 26° is only some 25 per cent. higher than at zero incidence.

A later determination of the drag at zero incidence in the Compressed Air Tunnel is also discussed in Appendix II. A somewhat lower figure, 82 lb., was found at conditions corresponding to full scale flight at 100 ft./sec.

The calculations of performance have been carried out on the general lines of R. & M. 1727[11] and include the effect on the rotor characteristics of the changes of blade incidence due to twisting under the aerodynamic and other forces. Important modifications were made however, in that the investigation was extended to include corrections for the following major approximations made in that report :—

(1) Neglect of the loss of lift at the tips of the blades.

(2) Use of a mean angle of geometrical pitch along the blade, instead of the exact formula giving its variation under twist from root to tip. (The minor importance of this approximation was however verified in R. & M. 1727 for two particular values of μ.)

(3) Neglect of the component of radial flow along the blades.

Furthermore, when these corrections had been made it was thought more satisfactory to work to the correct final value of the lift (equal to the weight of the aircraft less the vertical component of the airscrew thrust and net tail plane and body lift) adjusting the rotor speed as necessary, rather than to base the results, as in R. & M. 1727, on measured values of the rotor speed obtained in gliding tests. A detailed discussion of these calculations may be found in Appendix III. Curves showing the total power required for level flight and the proportion due to parasitic drag are given in Fig. 17 for the two cases of δ (assumed mean profile drag coefficient of the blade) 0·014 and 0·012. Also the corresponding curves for $\delta = 0{\cdot}014$ at reduced loading are shown.

The airscrew characteristics have been calculated on the basis of a recent analysis[12] of full scale tests of a series of airscrews. In conjunction with the known engine curves from the log book these enable the variation of thrust power with speed to be reduced. An allowance has to be made for the parasitic drag in the slipstream, which is estimated to be about 60 lb. of the total, leaving finally an available power at sea level as shown in Fig. 17.

[To face page 26

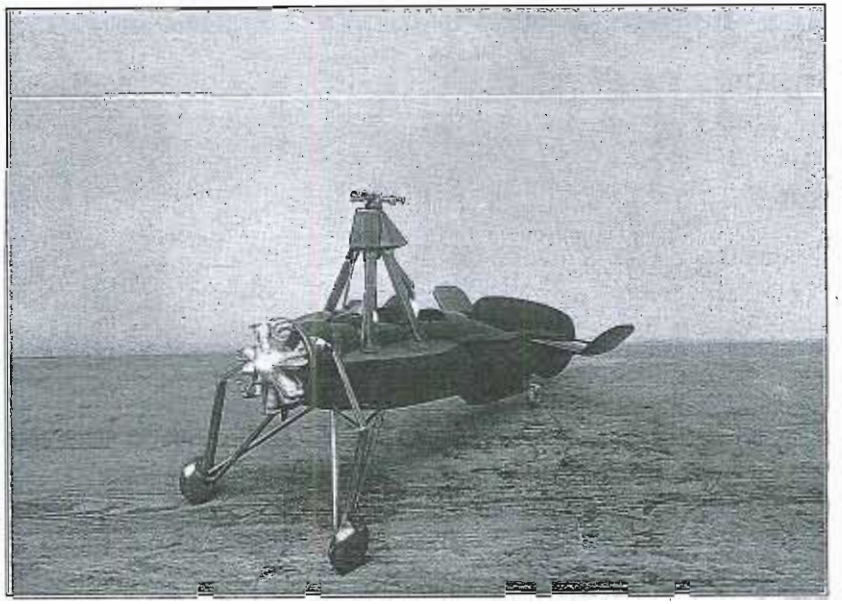

FIG. 16.—The Complete Model as Tested.

The intersections of the curves give the *maximum* and *minimum speeds* for level flight, which will be seen to be 91·5 and 36·5 m.p.h. respectively for $\delta = 0{\cdot}014$ or 94·5 and 35·0 m.p.h. for $\delta = 0{\cdot}012$. The *maximum rate of climb* is easily derived from the curves of Fig. 17 by subtracting the power required for level flight from the thrust power and thus obtaining the power available for climb. It is found to be 312 ft./min. for $\delta = 0{\cdot}014$ or 360 ft./min. for $\delta = 0{\cdot}012$, occurring respectively at indicated air speeds of 63·5 and 65·5 m.p.h.

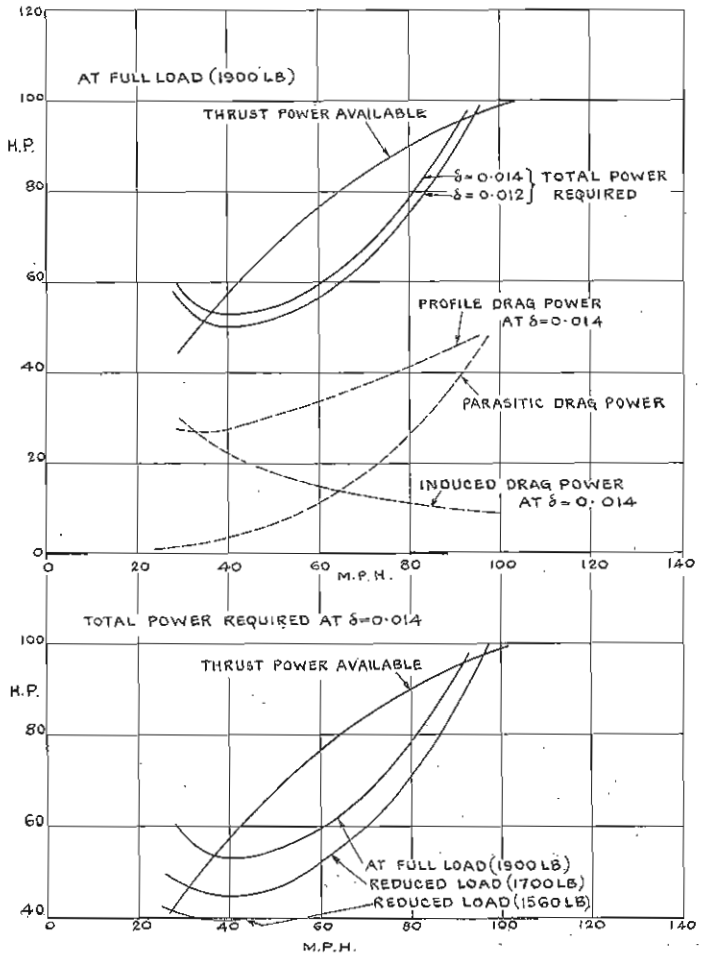

FIG. 17.—Performance curves.

The measured values in full scale flight tests (§5.1) were 94 and 32 m.p.h. for the maximum and minimum speeds and 355 ft./min. (at 57 m.p.h.) for the maximum rate of climb ; so that the present higher value of the parasitic drag, together with the more comprehensive calculation including blade twist, will give very satisfactory agreement with top speed and climb for $\delta = 0{\cdot}0123$ (a value which is lower than the $0{\cdot}014$ of R. & M. 1727 as might be expected, since in that report δ was assumed to include an empirical allowance for some of the above corrections). Although the agreement as regards minimum speed is not so good, this value of δ leading to a figure of $35{\cdot}2$ m.p.h., it should be remarked that the rotor is then at a somewhat high-angle-of-incidence-(about-15°)-where-the-basic-assumptions-of-the-rotor-theory cease to apply so accurately. Furthermore, the fuselage will not be so completely in the airscrew slipstream, which fact will decrease the drag ; and the slipstream will impinge more on the rotor, increasing the lift, so that on both counts the minimum speed is likely to be overestimated. Again, at the low speeds considered, the airscrew performance estimates are open to some doubt.

Reduction of the loading to 1,700 lb. gives new calculated figures of $96{\cdot}0$ and $30{\cdot}8$ m.p.h. for maximum and minimum speeds and 485 ft./min. for best rate of climb at $\delta = 0{\cdot}014$, and $98{\cdot}0$ m.p.h., $30{\cdot}0$ m.p.h. and 532 ft./min. at $\delta = 0{\cdot}012$. These compare fairly well with the measured performance 97 m.p.h., 28 m.p.h. and 540 ft./min., considering the large extent of the correction for rotor speed necessitated by this reduction of rotor thrust (*see* Appendix III, §13.4). At the further reduced loading, 1,560 lb., the minimum speed is calculated to be lower than that at full load by $9{\cdot}5$ m.p.h. (at $\delta = 0{\cdot}014$) as compared with measured reduction of $8{\cdot}5$ m.p.h. (to $23\frac{1}{2}$ m.p.h.).

For comparison with the aerodynamic tests, calculations were made on the gliding characteristics of the aircraft, assuming no thrust from the airscrew. (In this case a somewhat different thrust is required from the rotor than for level flight under power, involving a change of rotor speed. This was dealt with as described in Appendix III). Including the convenient multiplier μ^2, final lift and drag coefficient curves for $\delta = 0{\cdot}014$ and $\delta = 0{\cdot}012$ are compared in Fig. 18 with those deduced from the full scale tests, and the resulting gliding angle curve is shown in Fig. 19.

It will be seen that the resulting gliding angle is estimated too high at the low speed end and too low at high speeds, but the minimum of 10·5° (for $\delta = 0{\cdot}0123$) compares fairly well with the full scale value of 11°.

The results would agree better at high speed if an allowance were made for the drag of the airscrew, which was certainly far from zero in the flight tests.

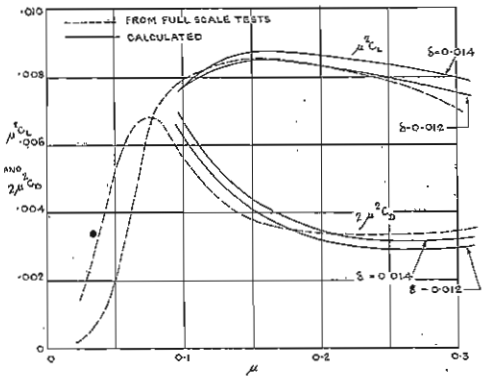

FIG. 18.—Overall lift and drag coefficients in gliding flight.

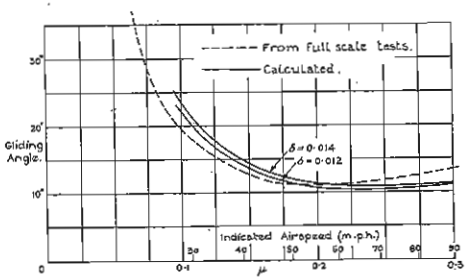

FIG. 19.—Gliding angle.

It is clear from these results that the rather poor performance of the C.30 autogiro could be greatly improved by a reduction of the parasitic drag. If by a general cleaning up of the structure the drag were reduced to half its present excessive value the top speed might be raised to 110 m.p.h. and the rate of climb improved some 50 per cent., without change of engine or airscrew.

6.2. *Rotor lift/drag ratio.*—A comparison is shown in Fig. 20 between the calculated and measured values of L/D for the rotor alone, the experimental points being obtained by subtraction of the appropriate parasitic drag as deduced from the

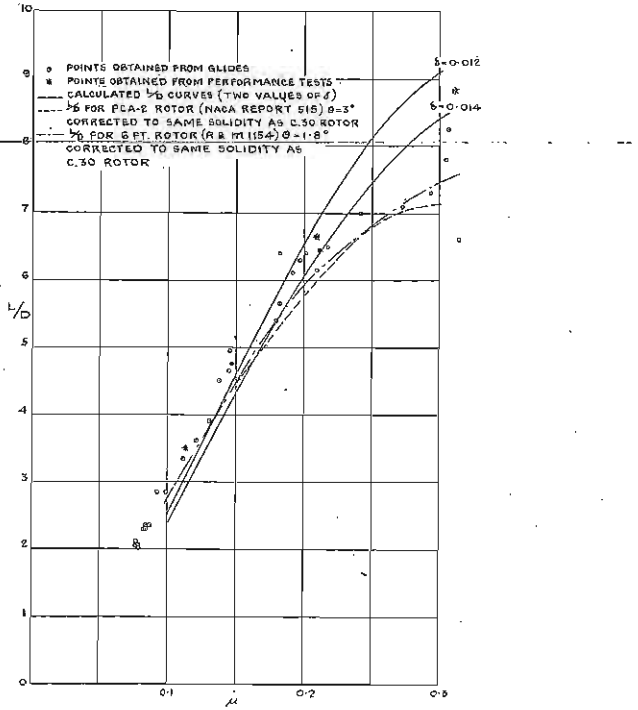

FIG. 20.—Measured L/D ratio for C.30 autogiro rotor compared with other rotors.

model tests and an allowance being made here for the drag of the airscrew. It will be seen that although the points derived from the performance tests agree at top speed with those calculated for $\delta = 0{\cdot}013$, the glides determine the rather lower value of 7·5 for L/D. Experimental results for an American rotor[13] and a 6-ft. model rotor,[5] when corrected by the method of R. & M. 1154[6] to the same solidity as the C.30, also gave a figure of this order (*see* Fig. 20), which would however be higher for the larger blade angle appropriate to the C.30 blades.

The dependence of the rotor L/D upon the solidity and blade angle, and the actual improvement that has taken place in this respect since the early days of the autogiro, are of considerable interest. In Fig. 21 the results of these calculations with typical values of these parameters are shown, in every case a value of 0·014

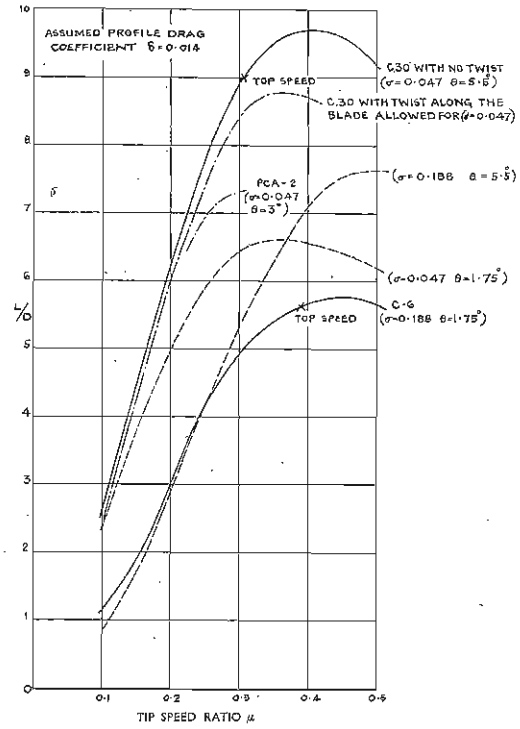

FIG. 21.—L/D for autogiro rotors (calculated)—effect of solidity and blade angle changes.

being assumed for the profile drag coefficient δ. (It may be remarked that recalculation at $\delta = 0{\cdot}012$ in general showed an increase of about 8 per cent. in L/D at the same value of μ.) The lowest curve is for a rotor with solidity four times that of the C.30 and blade angle about a third (of the untwisted value), and corresponds closely to the Cierva C.6 which was flown in 1925–6. The uppermost curve is that of the C.30 if no allowance is made for twist, which in practice reduces

the ratio to the chain dotted line. Maximum L/D was not reached in flight in either case, but it will be observed that the value at top speed (67 m.p.h., $\mu = 0{\cdot}39$ for the C.6; 94 m.p.h., $\mu = 0{\cdot}31$ for the C.30) has been increased from 5·6 to 9·0. As may be seen from the intermediate curves of which each corresponds to change of only one of σ and θ, the improvement at these speeds may be attributed equally to the two factors. In actual fact the advantage is not quite as marked as the above, since blade twist on the C.30, equivalent to a reduction in the mean blade angle, and an increase in blade thickness ratio from 12 per cent. in the C.6 to 17 per cent. on the C.30, which may give a decrease of 0·001 in the ϵ that should be assumed for the C.6, alter the respective figures for L/D to 5·9 and 8·8.

PART II

General blade motion in gliding flight

7. *Introductory.*—A theory of the twist of an autogiro blade in flight, and its effect on the rotor characteristics has been developed by Beavan and Lock.[11] This work has now been extended to cover the bending motion. Measurements have also been made in flight of the general blade motion, using a ciné camera mounted on the rotor head.

A short resumé of the results of the blade twist investigation, an account of the work on the blade bending, and the results of the measurements of the blade motion are contained in this part of the report.

8. *The effect of blade twist on the characteristics of the autogiro.*—In R. & M. 1727,[11] Beavan and Lock have analysed the blade motion and force characteristics of the C.30 autogiro rotor, taking into account the torsional flexibility of the blades. The analysis has been made over a range of speeds from zero to 130 m.p.h., using the physical constants of the blades, and assumed mean profile drag coefficients of 0·014 and 0·012.

The calculations show that the blade should twist to the extent of several degrees, in the sense that the mean pitch angle (at any radius) round the circle is decreased, and that superimposed on this there is a periodic variation. Both effects increase with the forward speed.

The most striking effects of twist are found in the rotor force characteristics (Fig. 22). In this figure, the rotor thrust has been deduced using measurements of rotor speed in the flight experiments (*see* Part I). Apart from the lower end of the speed range, where the rotor angular velocity upon which the calculations are based

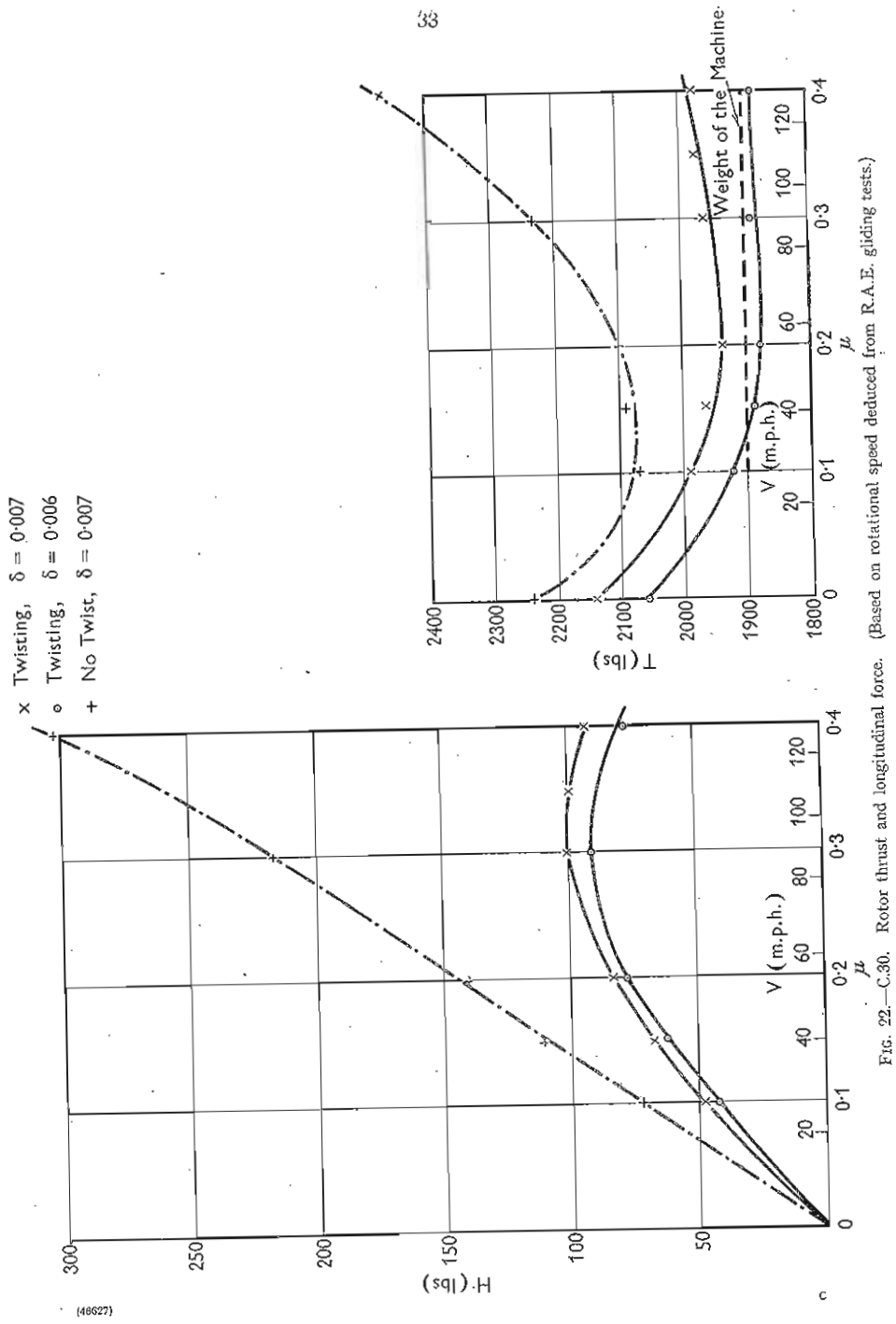

FIG. 22.—C.30. Rotor thrust and longitudinal force. (Based on rotational speed deduced from R.A.E. gliding tests.)

has had to be somewhat doubtfully extrapolated from the experimental curves, the twist results show a fairly constant thrust. Except at very steep angles of glide, the thrust should be approximately equal to the weight of the aircraft, and if the corrections of Appendix III for tip loss, etc., are made, fair agreement is obtained.

The changes in the rotor force characteristics due to the inclusion of twist, in particular the longitudinal force H, profoundly modify the pitching moment relationships, and also the control column position for equilibrium. It is known that the C.30 autogiro exhibits a curious reversal effect on the control column position to trim. To maintain steady flight at both high and low speeds the column has to be held further back (rotor tilted in the sense of greater incidence) than for the intermediate speeds (*see* the experimental points in Fig. 23). This may be considered to imply the existence of some form of instability, for since a backward movement of the control column always produces a nose up pitching moment, it follows that if the aircraft is flying in equilibrium at a fairly high speed and the speed then increases with the control column held fixed, a nose down pitching moment is produced which will tend to increase the speed still further. The phenomenon is qualitatively predicted on the twist theory, as is shown by Fig. 23, in which the angle χ between the rotor axis and the perpendicular to the body datum is plotted against μ. The remaining discrepancy there shown between the theoretical value and the approximate curve obtained in gliding tests is not considered serious, in view of the critical dependence of χ on the exact fore and aft position of the centre of gravity of the whole aircraft, and on the aerodynamic characteristics and downwash on the tail plane.

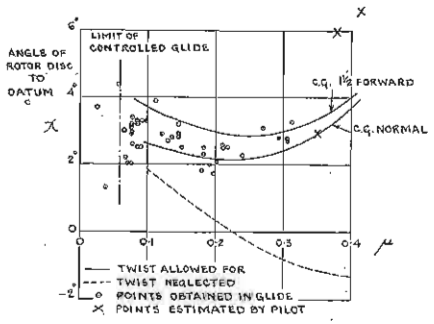

FIG. 23.—Control column—position for trim.

It is obvious that measurements of the blade twist and motion are of great interest as confirmation of the correctness of the assumptions made in this work. Comparisons made later in this part show agreement which is reasonably close, bearing in mind the difficulties of such measurements.

9. *Calculation of blade bending.* 9.1. *Introduction.*—In certain flights of autogiros of the C.30 type, a mechanical failure has developed in the rotor, usually occurring as a fracture in the spar or its associated members, at the root of the blade. Although it was thought improbable that the bending stresses on the blade in flight would be large enough to account for this, and some photographic evidence[14] seemed to support this conclusion, it was considered desirable to attempt some theoretical and practical approach to the problem of the magnitude of the bending under the ordinary conditions of steady flight. On the theoretical side the more detailed knowledge provided by recent mathematical work on the aircraft is useful in giving a firmer basis for the calculations. In the following treatment, in connection with which acknowledgments are due to Mr. Pugsley of the R.A.E. for some valuable advice, the theory and results of R. & M. 1727[11] are assumed throughout, and the notation of that report is adhered to.

9.2. *General.*—It is assumed initially, and verified subsequently by the numerical results, that whatever bending takes place is insufficient to affect the calculated values of the aerodynamic forces at any point of the blade to an appreciable extent. Also that the distance r from the hinge to an element of the blade, which is further considered uniform along its length, is unchanged to the first order of the bending.

It is convenient to discuss the bending as a departure of the blade from the instantaneous position it would have if it were infinitely stiff. For steady flight, as is here assumed, this latter is completely defined by ψ, the angle of rotation of the blade from its backward position, and β, the angle between the blade and the plane perpendicular to the rotor axis. But when the blade is bending it is necessary to define for each point of the blade an angle β' between the radius to the point and the aforesaid plane (*see* Fig. 24).

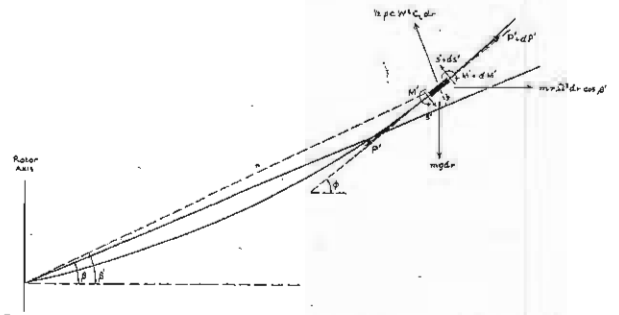

FIG. 24.—Forces on an element of blade in the plane through the rotor axis.

f then the upward deflection of the point r is y and the tangent to the blade (along :s length) is at an angle ϕ to the plane of rotation,

$$\begin{cases} \beta' = \beta + y/r & \ldots \quad (1) \\ \phi = \beta + dy/dr & \ldots \quad (2) \end{cases}$$

o the first order.

9.21. *Forces on an element* (*Fig.* 24).—The external forces on an element dr are hree, as far as concerns bending in the plane of the rotor axis. There is the lift $\rho c W^2 C_L dr$ acting perpendicularly to the datum "infinitely stiff" blade, the eight $mgdr$, and the centrifugal force $mr\Omega^2 dr \cos \beta'$ acting perpendicularly to he rotor axis.

Internal forces are S′ and S′ + dS′ the shear at the ends of the element, M′ and I′ + dM′ the bending moment, and P′ and P′ + dP′ the longitudinal tension along he blade. These latter give a component P′$d\phi$ perpendicular to the element.

Hence the equations of motion of the element perpendicular and parallel to itself re :—

$$mdr.r\,\ddot{\beta}' = \tfrac{1}{2}\rho c W^2 C_L dr \cos(\phi - \beta') - mr\Omega^2 dr \cos\beta' \sin\phi - mgdr\cos\phi + dS' + P'd\phi \quad \ldots \quad (3)$$

$$0 = mr\Omega^2 dr \cos\beta' \cos\phi - mgdr \sin\phi + dP' \quad \ldots \quad (4)$$

We have also, for the "infinitely stiff" datum :

$$mdr.r\,\ddot{\beta} = \tfrac{1}{2}\rho c W^2 C_L dr - mr\Omega^2 dr \cos\beta \sin\beta - mgdr\cos\beta + dS \quad (5)$$

Subtracting (5) from (3),

$$mdr.r\,(\ddot{\beta}' - \ddot{\beta}) = \tfrac{1}{2}\rho c W^2 C_L dr \left\{\cos(\phi - \beta') - 1\right\} - mr\Omega^2 dr(\cos\beta'\sin\phi - \cos\beta\sin\beta) - mgdr(\cos\phi - \cos\beta) + dS' - dS + P'd\phi \quad \ldots \quad (6)$$

Neglecting second order terms of the small angles β, β' and ϕ, and the gravity erm mg, in (4) and (6),

$$\begin{cases} 0 = mr\Omega^2 dr + dP' & \ldots \quad (7) \\ mdr.r\,(\ddot{\beta}' - \ddot{\beta}) = -mr\Omega^2 dr(\phi - \beta) + dS' - dS + P'd\phi & \ldots \quad (8) \end{cases}$$

Hence, remembering that P′ is zero at the free end R of the blade : —

$$P' = \tfrac{1}{2}m\Omega^2(R^2 - r^2) \quad \ldots \quad (9)$$

And, from (1) and (2) in conjunction with (8) :

$$m\ddot{y} = -mr\Omega^2\frac{dy}{dr} + \frac{dS'}{dr} - \frac{dS}{dr} + \tfrac{1}{2}m\Omega^2(R^2 - r^2)\frac{d^2y}{dr^2} \quad (10)$$

9.22. *Differential equation of bending.*—By considering the rotational equilibrium of the element one may obtain in the normal way :—

$$S' = \frac{dM'}{dr} = -EI\frac{d^3y}{dr^3}$$

Hence, substituting and re-arranging :—

$$EI\frac{d^4y}{dr^4} - \tfrac{1}{2}m\Omega^2(R^2 - r^2)\frac{d^2y}{dr^2} + mr\Omega^2\frac{dy}{dr} + m\ddot{y} = -\frac{dS}{dr} \quad \ldots \quad (11)$$

Putting $x = r/R$ and $K = mR^4\Omega^2/2EI$ this differential equation for bending becomes finally

$$\frac{d^4y}{dx^4} - K(1 - x^2)\frac{d^2y}{dx^2} + 2Kx\frac{dy}{dx} + \frac{2K}{\Omega^2}\frac{d^2y}{dt^2} = -\frac{R^4}{EI}\frac{dS}{dr} \quad \ldots \quad (12)$$

9.23. *The applied forces.*—The term on the right hand side of equation (12) is a blade loading which may be obtained from data, such as in R. & M. 1727,[11] of the flapping and twisting of the blades. It may be evaluated as follows (for the case of an assumed mean angle of pitch along the blade, as in R. & M. 1727) :

From the values of λ, a_0, a_1, b_1, θ_0', θ_1 for a given value of μ and Ω work out as functions of x and ψ only (otherwise numerical) :

$$\theta = \theta_0' - \theta_1\sin\psi$$

$$U_X = xR\Omega + \mu R\Omega\sin\psi$$

$$U_Y = \lambda R\Omega - xR(a_1\sin\psi - b_1\cos\psi) - \mu R\Omega a_0\cos\psi + \mu R\Omega a_1\cos^2\psi + \mu R\Omega b_1\sin\psi\cos\psi.$$

Thus obtain as a function of x and ψ

$$\frac{dS}{dr} = c\rho a(U_X U_Y + \theta U_X^2) - mR\Omega^2 a_0 x - mg$$

which is effectively a reduced form of equation (5) of R. & M. 1127[4].

Reduce the terms $\sin^2\psi$, $\sin^3\psi$, $\sin\psi\cos\psi$, $\cos^2\psi$ . . . . to the first power forms $\sin\psi$, $\sin 2\psi$, $\sin 3\psi$ . . . . $\cos\psi$, $\cos 2\psi$ . . . . and in accordance with the general principle of R. & M. 1727 neglect all but those in $\sin\psi$ and $\cos\psi$.

Hence obtain the load grading in the form

$$-\frac{R^4}{EI}\frac{dS}{dr} = (a_1x^2 + b_1x + c_1) + (a_2x^2 + b_2x + c_2)\sin\psi + (a_3x^2 + b_3x + c_3)\cos\psi \quad \ldots \quad (13)$$

A valuable check on this arithmetical work is afforded by the fact that the moment of this loading about the hinge should be zero for all values of ψ. This requires

$$\int_0^1 x(a_1x^2 + b_1x + c_1)\,dx = \int_0^1 x(a_2x^2 + b_2x + c_2)\,dx = \int_0^1 x(a_3x^2 + b_3x + c_3)\,dx = 0, \text{ or } \frac{1}{4}a_1 + \frac{1}{3}b_1 + \frac{1}{2}c_1 = 0, \text{ etc.}$$

further calculations were made to this order of accuracy. Curves showing the rapidity of the approximations in this and other problems may be found in R. & M. 1799.[15] It should be noted that such a five point collocation solution merely includes powers of x up to x^8, the first few of these being little different from those in the complete exact infinite series (cf. Table 7).

TABLE 7

Solutions of $\frac{d^4y}{dx^4} - 49\,(1-x^2)\,\frac{d^2y}{dx^2} + 98x\,\frac{dy}{dx} = 307x^2 - 215x - 10{\cdot}17$

	By Collocation.			Exact.
	3-point.	4-point.	5-point.	
$y =$	$-0{\cdot}1503x$ $+0{\cdot}9930x^2$ $-0{\cdot}4240x^4$ $-0{\cdot}3854x^5$ $+0{\cdot}2278x^6$	$-0{\cdot}2061x$ $+0{\cdot}6051x^3$ $-0{\cdot}4236x^4$ $+0{\cdot}7019x^5$ $-0{\cdot}9117x^6$ $+0{\cdot}3515x^7$	$-0{\cdot}2307x$ $+0{\cdot}6999x^3$ $-0{\cdot}4236x^4$ $-0{\cdot}1279x^5$ $+0{\cdot}6273x^6$ $-0{\cdot}7293x^7$ $+0{\cdot}2724x^8$	$-0{\cdot}2290x$ $+0{\cdot}6863x^3$ $-0{\cdot}4236x^4$ $+0{\cdot}0767x^5$ $+0{\cdot}1609x^6$ $-0{\cdot}3909x^7$ $+0{\cdot}3875x^8$ $-0{\cdot}3033x^9$ $+0{\cdot}1455x^{10}$ $+0{\cdot}0003x^{11}$ $-0{\cdot}0612x^{12}$ $+0{\cdot}0780x^{13}$ $-0{\cdot}0491x^{14}$ $+0{\cdot}0182x^{15}$ $+0{\cdot}0007x^{16}$ $-0{\cdot}0089x^{17}$ $+0{\cdot}0070x^{18}$ $-0{\cdot}0036x^{19}$ $+0{\cdot}0008x^{20}$ $+0{\cdot}0005x^{21}$
$\int_0^1 xy\,dx$	0·0512	0·0071	−0·0012	−0·0000[6]
Value of y at $x = 0$	0	0	0	0
$\frac{1}{4}$	−0·0241	−0·0431	−0·0485	−0·0482
$\frac{1}{2}$	0·0140	−0·0434	−0·0531	−0·0523
$\frac{3}{4}$	0·1210	0·0179	−0·0006	+0·0017
1	0·2611	0·1171	0·0881	0·0928

9.4. *Bending of rotor blades.*—A few typical cases have been worked out, namely $\mu = 0, 0{\cdot}2$ and $0{\cdot}3$. The data, derived from R. & M. 1727[11], and the solutions, evaluated at various points of the range are listed in Table 8. Fig. 25 shows the results plotted as blade deflection from the "infinitely stiff" datum, and in Fig. 26 the various components y_1, y_2 and y_3 are shown separately, all being here reduced to a basis given by the line joining the root to the tip.

TABLE 8

Values of y at points along the blade

$y = y_1 + y_2 \sin\psi + y_3 \cos\psi$; where y_1, y_2, y_3 satisfy the differential equations (14), (15) and (16) for the following values of the coefficients:

μ	K	a_1	b_1	c_1	a_2	b_2	c_2	a_3	b_3	c_3
0	49·1	307	−215·0	−10·17	0	0	0	0	0	0
0·2	52·1	306	−226·3	− 2·11	−177·5	122·1	7·35	125·2	− 95·0	0·73
0·3	61·0	324	−251·0	5·33	−272·0	194·0	6·67	183·0	−142·5	3·50

	$\mu = 0$	$\mu = 0{\cdot}2$			$\mu = 0{\cdot}3$		
	y_1	y_1	y_2	y_3	y_1	y_2	y_3
$x = 0$	0	0	0	0	0	0	0
$\frac{1}{4}$	−0·0485	−0·0420	−0·0060	0·0031	−0·0355	−0·0074	0·0036
$\frac{1}{3}$	−0·0561	−0·0490	−0·0138	0·0071	−0·0416	−0·0166	0·0084
$\frac{1}{2}$	−0·0531	−0·0467	−0·0402	0·0225	−0·0404	−0·0505	0·0283
$\frac{3}{4}$	−0·0007	0·0003	−0·1118	0·0654	−0·0003	−0·1426	0·0792
1	0·0881	0·0783	−0·2076	0·1235	0·0701	−0·2682	0·1524

It appears that the flexure of the blade nowhere amounts to more than about 2 in., which on a length of 18·5 ft. means that the bending stresses are negligible.

Since the curves of deflection in Fig. 26 are nearly symmetrical it seems that the larger bending moments one might expect on the inner parts of the blades towards the hinges are nullified by the extra stiffness due to the greater centrifugal tension there.

As might be expected the periodic component of bending increases with speed, though not uniformly. The permanent deflection however decreases.

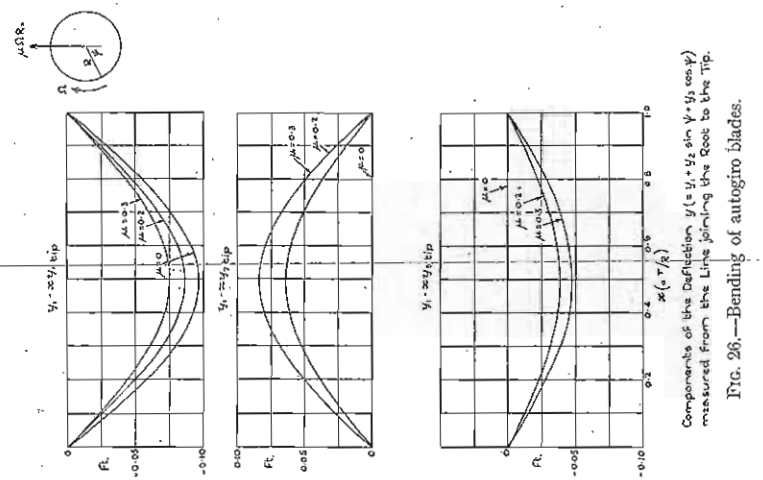

Components of the Deflection, $y_1 = y_1 + y_2 \sin\psi + y_3 \cos\psi$, measured from the Line joining the Root to the Tip.

FIG. 26.—Bending of autogiro blades.

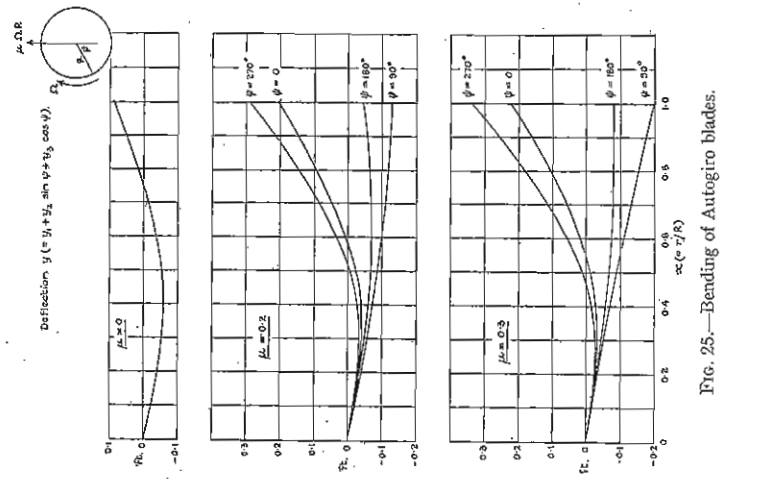

FIG. 25.—Bending of Autogiro blades.

10. *Measurement of blade motion in steady flight.* 10.11. *Description of camera installation.*—A ciné camera, taking 30–40 pictures a second on 9·5 mm. film, was mounted above the rotor-head, and rotated with it. The camera was adjusted to point along a blade, and was pitched up about 1·5° from the plane perpendicular to the rotor axis (Fig. 27). The camera was started and stopped by an armature and solenoid, energised with current picked up by two slip-rings on the rotor head, from brushes fixed to the pylon. A third slip-ring, only half of which was conducting, operated an indicating mechanism defining the position of the blade in

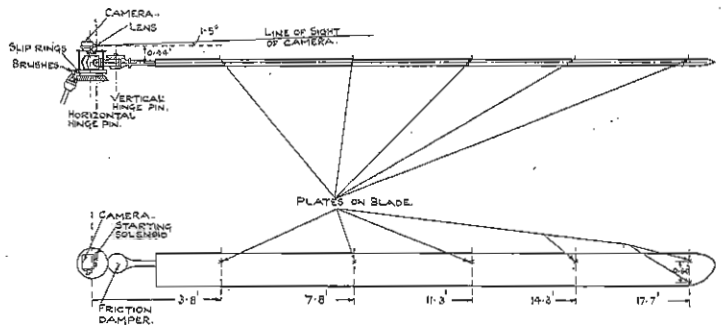

FIG. 27.—Arrangement of camera and plates on blade.

azimuth. This consisted of a small pointer which had two positions in the frame of the picture. When the conducting half of the slip-ring was in contact with the brush on the pylon, the pointer took up one position, and dropped back to the other position when the non-conducting half of the slip-ring was in contact with the brush. The only information obtained directly from this indicator was, therefore, whether the blade was on the port or the starboard side.

To record the position of the blade, small plates of dural $\frac{3}{16}$ in. × $\frac{3}{16}$ in. were fixed to the blade which was to be photographed. The position of these plates is shown in Fig. 27. The three blades were re-balanced after the plates had been mounted.

10.12. *Method of test.*—Before each flight a sight, fitted to the rotor head, was photographed to check the setting of the camera.

Steady glides were made at seven different speeds, and instrument readings taken as in the normal glide tests. These readings defined the working condition of the rotor. The camera was switched on for about 10 seconds half way through the glide.

The film was projected, giving an image of about 6 in. × 9 in. Enlargements of actual pictures are given in Figs. 28 (*a*) and (*b*), showing the position and the appearance of the blade at two azimuth angles. The positions of the plates relative to the mask of the picture were measured ; from the photographs of the sight taken before the flight, the positions of the points were obtained relative to the trace on the picture of the plane perpendicular to the rotor axis. Points along the spar-line of the blade gave flapping, coning and bending, the displacement between points on the trailing edge and corresponding points on the spar-line gave the blade incidence which provided a measure of the twist at the section. The measured distance apart of corresponding points gave the camera magnification.

About sixty pictures were measured corresponding to about five revolutions of the rotor head. By assuming constant camera speed, it was possible to calculate the azimuth angle of any frame. The positions of the plates, and the blade angles were plotted against azimuth angle, on a base of 0° to 360°, the results from different revolutions being superimposed. Figs. 29 (*a*) and (*b*) give examples of the points obtained for motion of the blade perpendicular to, and in, the plane of rotation.

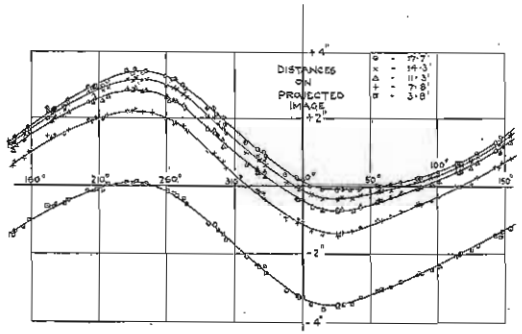

FIG. 29*a*.—Measured distances on projected image against azimuth angle. Motion perpendicular to plane of rotation.

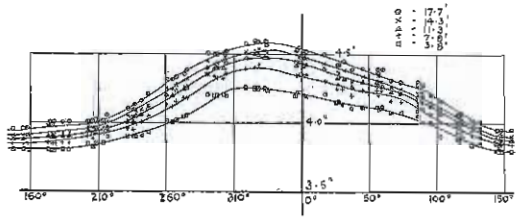

FIG. 29*b*.—Measured distances on projected image against azimuth angle. Motion in plane of rotation.

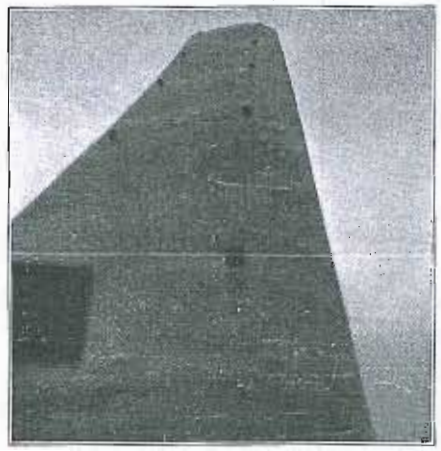

FIG. 28 (*a*).—Enlargement of specimen picture.
$V_i = 90$ m.p.h. $\psi = 260°$

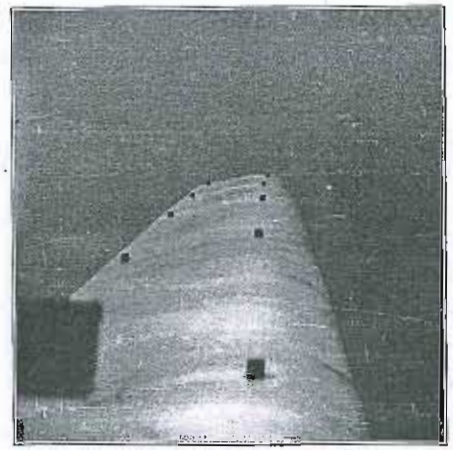

FIG. 28 (*b*).—Enlargement of specimen picture.
$V_i = 90$ m.p.h. $\psi = 80°$

Mean curves drawn through the points were then analysed by Runge's method[16] to give Fourier coefficients. An example is given in Fig. 30 which compares the curves obtained for blade incidence at 90 m.p.h., by taking in succession the constant term, constant term and first harmonic, and finally constant term, first harmonic and second harmonic, with the measured blade incidences at various azimuth positions.

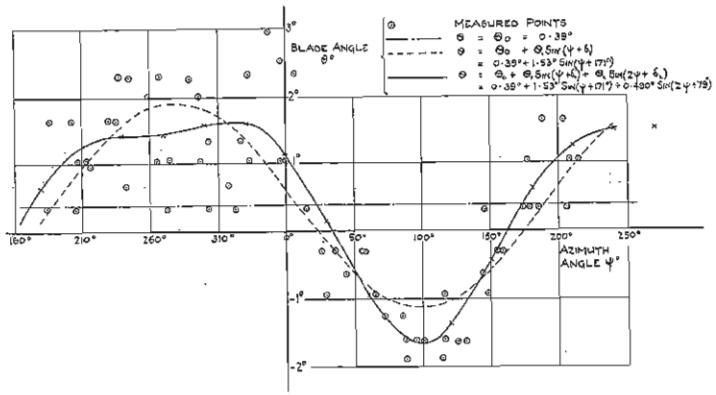

FIG. 30.—Comparison of measured blade angles $\theta°$ with Fourier series representing them.
Tip section, $V_1 = 90$ m.p.h. $\mu = 0{\cdot}313$.

10.13. *Accuracy.*—There were two serious disadvantages in the method used. The first was that no positive external datum from which to measure the plate-positions had been included in the picture. This was overcome by using the mask line of the picture as a reference, and comparing this with the measured height of the sight photographed on the ground.

The second disadvantage was that no definite indication of azimuth angle was given, and due to the varying speed of the camera, the azimuth angle may be in error by $\pm 10°$. It was therefore decided to plot magnitudes and phase angles instead of the usual coefficients of the Fourier series.

The position of the plates could be read to an accuracy corresponding to about $0{\cdot}05°$ in angular movement, and about 0·02 ft. at the blade tip. Jump of the mask in the camera or of the camera in its supports could certainly cause apparent movements of the blade exceeding this.

Bending deflections were measured by comparing the relative motion of two points on the blade. Movement of the mask in the camera would not affect this

and the probable error is $\pm 0{\cdot}05$ ft. at the tip, or $\pm 0{\cdot}025$ ft. at the mid-section. A consistent error in the permanent bending deflection may occur, as this involves the height of the camera above the blade, which could not be measured accurately.

The relative deflection of the points on the sparline and the trailing edge could be measured to an accuracy equivalent to $\pm 1{\cdot}5°$ at the tip. The accuracy of the mean curve, and of the coefficients will be higher, and possibly the value of the coefficients will be within $\pm 0{\cdot}5°$.

10.2. *Results.* 10.21. *General definitions.*—Fig. 31 gives the conventions of measurement of the various quantities referred to in this section. The actual results have been cast into the following form for the reasons given above.

(*a*) Coning and flapping motion perpendicular to the plane of the disc : the angle $\beta°$ which the line joining tip and root of the blade makes with the plane perpendicular to the rotor axis (Fig. 31*a*), is given by

$$\beta° = A_0 + A_1 \sin(\psi + \psi_1) + A_2 \sin(2\psi + \psi_2) + A_3 \sin(3\psi + \psi_3)^*$$

(*b*) Motion in the plane of the disc : the angle $\zeta°$ which the projection of the line joining tip and root of the blade in the plane perpendicular to the rotor axis makes with the mean position of this projection (Fig. 31*b*) is given by

$$\zeta° = \mu_1 \sin(\psi + \delta_1) + \mu_2 \sin(2\psi + \delta_2) .$$

(*c*) Pitch angle of the blade : the angle $\theta°$ which the chord line of a section makes with the plane perpendicular to the rotor axis (Fig. 30) and which therefore measures the twist is given by

$$\theta° = \theta_0 + \theta_1 \sin(\psi + \gamma_1) + \theta_2 \sin(2\psi + \gamma_2) .$$

All the above coefficients are given in degrees.

(*d*) Bending of blades : the deflection y of a point on the blade distance r from the root, above the line joining tip and root of the blade (Fig. 31*a*), is given by

$$y = Y_0 + Y_1 \sin(\psi + \varepsilon)$$

Y_0, Y_1 are given in ft., and are functions of the quantity $x = \frac{r}{R}$.

* In terms of the usual Fourier coefficients,

$$A_0 = a_0, \quad A_1 = \sqrt{a_1^2 + b_1^2}, \quad A_2 = \sqrt{a_2^2 + b_2^2}, \quad A_3 = \sqrt{a_3^2 + b_3^2}$$

$$\psi_1 = \tan^{-1}\frac{a_1}{b_1}, \qquad \psi_2 = \tan^{-1}\frac{a_2}{b_2}, \qquad \psi_3 = \tan^{-1}\frac{a_3}{b_3}$$

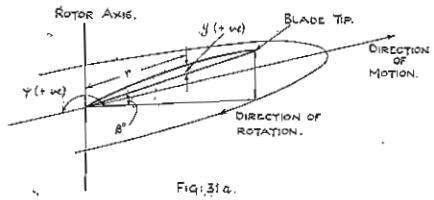

FIG. 31*a*.

CONVENTIONS FOR MEASUREMENT OF AZIMUTH ANGLE Ψ
CONING & FLAPPING ANGLE β
& BENDING y

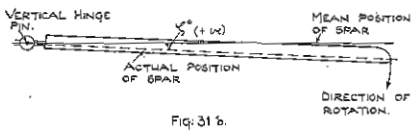

FIG. 31*b*.

CONVENTION FOR MEASUREMENT OF THE MOTION IN THE PLANE OF THE DISC ζ

FIG. 31.—General conventions of measurement.

The measured coefficients are compared below with those based on calculations. The mechanical constants of the blade have been measured and the results summarised in Table 9.

TABLE 9

Characteristics of rotor blade which was used for measurement of blade twist and bending

Chord, C	0·917 ft.
Tip radius, R	18·5 ft.
Mass of blade/unit length, m	0·0615 slug/ft. run.
Distance of C.G. behind spar axis, b	0·06 ft.
Geometrical pitch at root, θ_n	0·0465 radians.
Pitching moment coefficient about the spar axis, C_m	−0·052.
Torsional stiffness (NJ)	19,900 lb. ft./radian/ft. run of blade.
Bending stiffness (EI)	27,900 lb. ft.^{2}

10.22. *Coning and flapping motion.*—Fig. 32 shows the magnitude of the coning and flapping motion at the tip, and Fig. 33 the phase angles, plotted against the tip speed ratio μ. Theoretical curves,[11] including and neglecting the effect of twist,

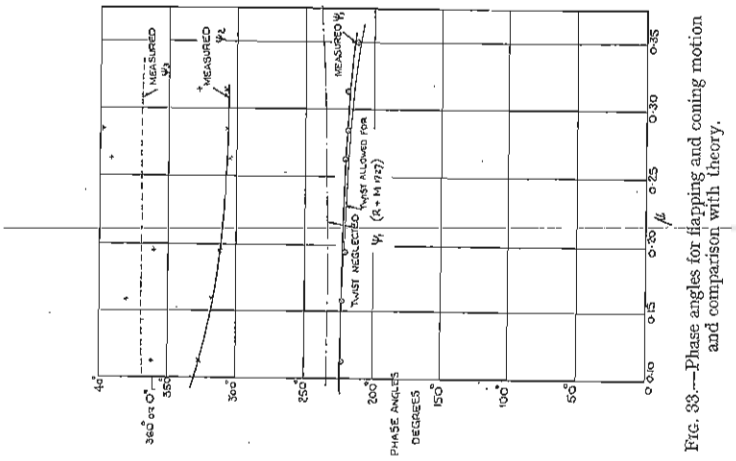

FIG. 33.—Phase angles for flapping and coning motion and comparison with theory.

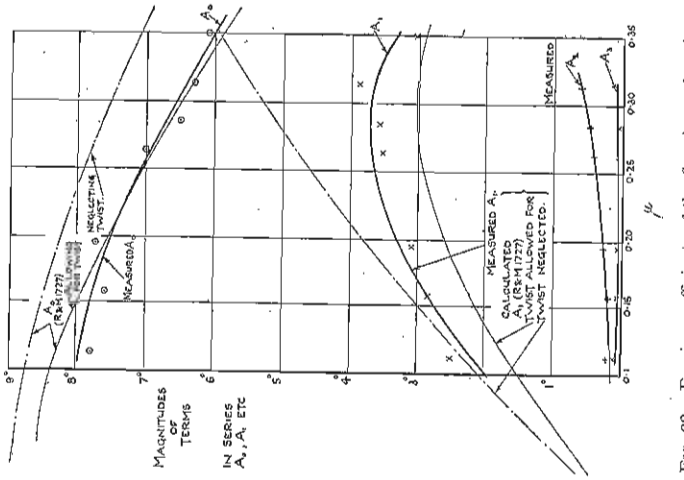

FIG. 32.—Fourier coefficients of the flapping and coning motion and comparison with theory.

are also given for the constant term and the first harmonic. Good general agreement is found with the theoretical curves (including effect of twist) for the magnitude of the coning motion (A_0) and the phase angle of the flapping motion (ψ_1). The magnitude of the first harmonic of blade motion A_1 is rather higher than the theoretical magnitude, including blade twist, but not so high as the theoretical curve, neglecting blade twist. The general form of the measured curve agrees with that of the theoretical curve, including blade twist, and shows the reduction of the magnitude of flapping motion beyond a value of $\mu = 0{\cdot}30$.

10.23. *Motion in the plane of the disc.*—Fig. 34 shows the variation with tip speed ratio of the magnitudes and phase angles of the first and second harmonics of blade motion in the plane of the disc. A comparison has been made of the first harmonic with that calculated using considerations of angular momentum alone.[17] It appears that this method gives a sufficiently close approximation to the actual motion.

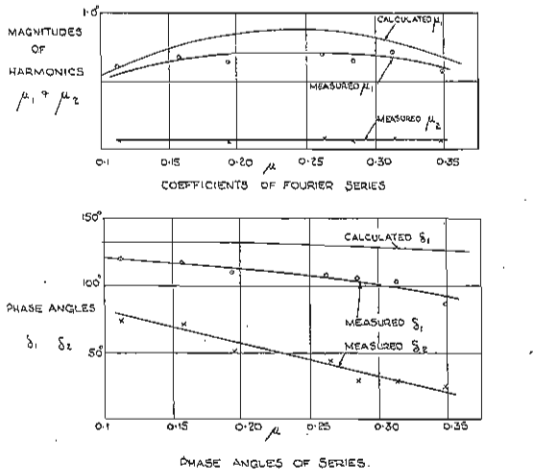

FIG. 34.—Coefficients and phase angles of Fourier series representing blade motion in plane of disc.

10.24. *Blade twist.*—Fig. 35 shows the magnitude of the coefficients and the phase angles defining the blade pitch angle at the tip, plotted against tip speed ratio μ. Excellent agreement with theory[11] is generally obtained.

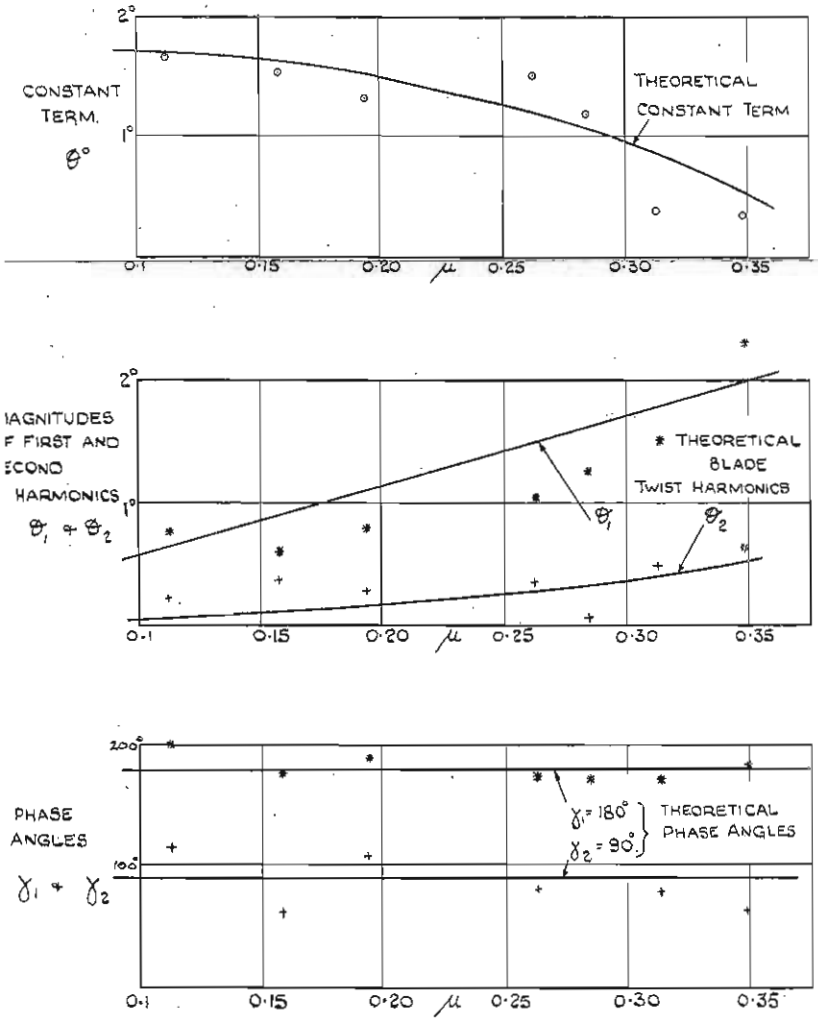

FIG. 35.—Coefficients and phase angles of Fourier series representing pitch angle at the tip section, and comparison with theory.

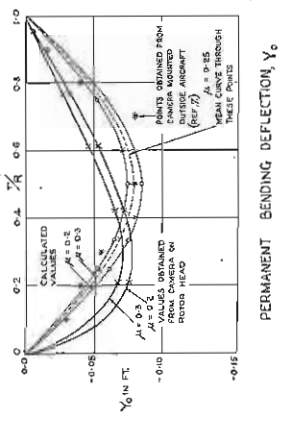

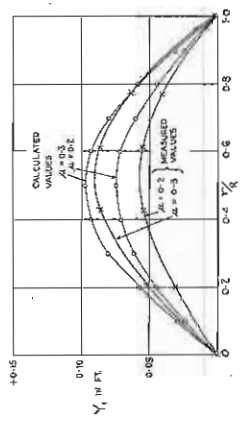

FIG. 37.—Comparison of measured and calculated bending deflections. $y = Y_0 + Y_1 \sin(\psi + \epsilon)$.

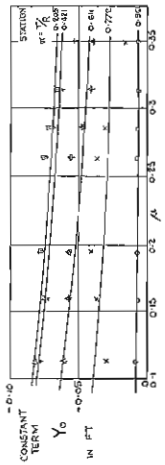

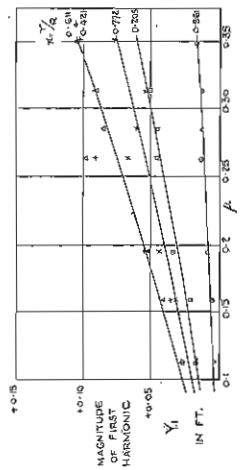

FIG. 36.—Deflection of blade at various stations expressed in form $y = Y_0 + Y_1 \sin(\psi + \epsilon)$.

10.25. *Blade bending.*—In Fig. 36 are given the coefficients defining the measured deflection perpendicular to the blade at various stations along it, plotted against tip speed ratio μ. Faired curves have been drawn through the points, and Fig. 37 is the result of cross-plotting from these curves at tip speeds of $\mu = 0{\cdot}2$ and $0{\cdot}3$, for comparison with theory (§9.4).

The permanent deflection curve is found to be asymmetrical, having a maximum for $\mu = 0{\cdot}3$ of $-0{\cdot}07$ ft. at $0{\cdot}30$R from the rotor axis; the theoretical maximum for this value of μ is $-0{\cdot}075$ ft. at $0{\cdot}50$R. The periodic deflection curve has a measured maximum of $0{\cdot}09$ ft. at $0{\cdot}5$R, and a calculated maximum of $0{\cdot}095$ ft. at $0{\cdot}5$R, for a μ of $0{\cdot}3$. Calculated and measured curves agree in that the permanent bending deflection decreases with increase of tip speed ratio, while the periodic bending deflection increases.

The average value of the phase angle ε for all values of μ and $\varkappa$ is $-28°$. The maximum deflection of the blade round the disc occurs at an azimuth angle of 298°.

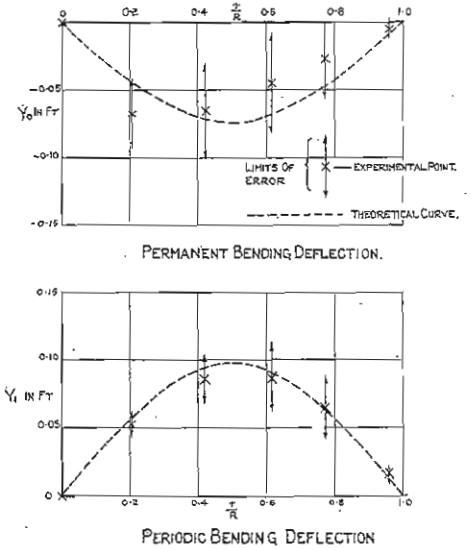

FIG. 38.—Comparison of theoretical bending curves with observed points, with limits of error of observation shown.

Some photographs showing blade bending had been obtained previously using a ciné-camera external to the autogiro[14]. One of these photographs was measured

to give the deflection along the blade; in this photograph the azimuth angle was 30°, so that using a phase angle of −28° for the periodic bending deflection, the deflection curve corresponds approximately to the permanent bending deflection curve alone. The resulting curve is plotted in Fig. 37 for comparison with the present results, and agrees closely with the theoretical curves. In view of this, the lack of agreement between the measured permanent deflection obtained in the later measurements, and the theoretical permanent deflection, may be due to a consistent error in the measured values. Such an error, as discussed in §10.13, could arise in the permanent bending deflection, though not in the periodic bending deflection.

In Fig. 38 curves of bending deflection against blade length are replotted, and the limits of error shown. It will be seen that the calculated curves lie within the region defined by the amount of possible error.

Measurements were also made of the bending of the blade in the plane of rotation. It was found to be negligibly small.

11. APPENDIX I

Pilot's notes on flying the direct control autogiro

11.1. *Foreword.*—When the vast majority of a pilot's flying is done in aeroplanes and but a small fraction in direct control autogiros it is hard to refrain from drawing a comparison between the two in which an allowance is made for their rather different flying characteristics. This is unfair to both the aeroplane and the autogiro and an attempt will be made, so far as is possible, to avoid comparison with the aeroplane and to confine remarks to considerations of the direct control as a means of manœuvring the autogiro.

11.2. *Reactions of aeroplane pilot.*—At the outset, however, it is necessary to refer to the aeroplane to explain the reactions of an aeroplane pilot flying an autogiro for the first time. Some pilots have an instinctive desire to move the control column in the wrong direction at first. This is because, though the hand moves in the same way as in an aeroplane, the control column tilts in the opposite direction. This desire is soon overcome.

Just before take-off and during the last stages of landing the feet have to be kept on the tail wheel steering bar (to keep the autogiro straight during the take-off run and after landing), which leads to an overwhelming desire to steer by the feet instead of by the hand on the control column. This is a desire which persists, when checking drift during a landing, even after some fifty hours' flying on the autogiro.

It is only natural therefore that the rudder is missed. When well in the air the feet may be removed from the tail wheel steering bar and the desire to move the legs in sympathy with the control column is greatly reduced.

11.3. *Control within normal speed range.*—The normal speed range is the range within which the flying characteristics do not greatly differ from those of the aeroplane, and within this range the autogiro is very simple to handle. There is a good deal of lag in the fore and aft control, though practically none in the lateral control. The control is rather heavy, especially in turns. Turns up to about 45 degrees of bank are possible, but if the bank is increased beyond this, the nose drops and a spiral commences in which the speed increases rapidly, making it necessary to reduce the angle of bank before the safe limit is passed. No other manœuvres can be performed within this speed range.

Owing, presumably, to gyroscopic action, on pulling back the control column, the autogiro tends to swing to the right as the nose rises, and on pushing forward the column the aircraft tends to swing to the left as the nose falls. In both cases the rate of swing is roughly proportional to the rate of rise or fall of the nose. If the throttle is suddenly closed the autogiro tends to swing to the left, and on rapidly opening the throttle, to the right.

In level flight the fore and aft bias, which is very effective, can be set so that only small forces are required on the stick to keep longitudinal trim.

There is a side force on the control column which varies with speed, and this can be neutralised by adjustment of the lateral bias control. When trimmed laterally, for speeds below about 40 m.p.h. (A.S.I.) the autogiro tends to swing to the left on releasing the control, and for speeds above this it tends to swing to the right. This occurs with engine on or off.

Even in still air the autogiro cannot be flown hands off for any length of time, and in average bumps it is definitely unstable. Fortunately its departures from a given attitude occur slowly, and the necessary adjustment of the control column can be made in a very leisurely fashion. Bumps of average magnitude make the autogiro wallow and swing in a pendulum-like manner about the rotor head, but no sharp accelerations are transmitted to the fuselage, and no undue jerking is felt on the control column.

11.4. *Flight above and below normal speed range.*—Outside the normal speed range the autogiro is not so easy to handle as might at first be expected. The characteristics will be discussed under the following sub-headings.

(*a*) *High speed.*— Up to about 115 m.p.h. the nose has to be forced down, but beyond this speed the autogiro becomes nose heavy. As the speed increases the nose heaviness increases, and the height lost in regaining level flight becomes unduly large. This is due rather to the extremely sluggish response to control movement than to the force required to move the control. It seems, and this is well supported by evidence, that beyond a certain speed it becomes very difficult, if not impossible, to recover from a dive. The specified maximum permissible speed must, therefore, not be exceeded.

(*b*) *Slow flying.*—Slow flying close to the ground, besides being a matter of practice, requires an understanding of the limitations imposed by the following four facts :—

(i) For a given throttle setting, the increase in the rate of climb for an increase in speed above minimum level speed is small, and less than the increase in the rate of descent for the same decrease in the speed below minimum level speed.

(ii) There is a large time lag in the fore and aft control.

(iii) The control column cannot be pushed forward too quickly to increase speed or the autogiro will sink bodily on to the ground before it has had time to change its attitude (*i.e.* get nose down a bit) and increase speed.

(iv) The lag in the lateral control is small but a fairly large angle of bank and a certain amount of sideslip have to be reached before the aircraft begins to turn.

The cumulative effect of (i), (ii) and (iii), in straight flight is that the fore and aft control cannot bring about the necessary adjustments in attitude and speed quickly enough to compensate for bumps. Thus to maintain level flight, adjustments of throttle setting have to be combined with control movements. As the mean throttle setting more nearly approaches full throttle, so must the height above the ground be increased if the possibility of an involuntary landing is to be eliminated, since even in absolutely smooth air, it is impossible to increase speed and commence to climb from full throttle minimum level speed without a small initial loss of height. The safe height for slow flying at full throttle naturally varies with the air conditions. In smooth air over level ground, 5 ft. is probably safe, while in bumps 15 to 20 ft. is more like the figure.

If it is necessary to turn during slow flight near the ground, the effect of (iv) in combination with (i), (ii) and (iii) has to be considered. A turn cannot be made without sideslip, which means losing a certain amount of height unless the throttle opening can be increased or a little forward speed gained. Thus, provided there is sufficient throttle opening in hand, slow turns can be made a few feet from the ground, but as the mean throttle opening becomes larger the height must be increased. If flying as slowly as possible at full throttle, it is impossible to turn without losing height.

(*c*) *Steep descent.*—Provided the airspeed is not excessively low, steep descent, with or without engine, presents no peculiar difficulty. Changes in throttle setting or alterations in pitch produce a slight yaw. When the forward speed falls to a certain limit (dependent on the load) the lateral control ceases to be effective, and the autogiro swings quickly to the right through about 180° and drops its nose. To regain control the column has to be eased forward. If it is held back, the nose rises again, speed is lost, and the swing is repeated. If this is done at full throttle the nose will be up at a steep angle and the manœuvre then becomes practically a stalled turn. At very low speeds the autogiro becomes tail heavy. With the engine on, the tail heaviness is likely to overpower the control, and unless the throttle is closed, full forward movement of the control column will not prevent the nose rising until lateral control disappears and an unpleasant stalled turn to the right occurs.

(*d*) *"Vertical" descent.*—If the control column is used vigorously in the following manner, nearly vertical descents with engine off appear possible. The speed is gradually reduced and the A.S.I. watched. As the speed at which the swing to the right occurs is approached, the column will have to be moved more and more to the left to keep the autogiro straight. The latter will become increasingly tail heavy. Finally the limit of lateral control column movement is reached and the autogiro will begin to swing to the right. Immediately this happens the column should be pushed hard up against the instrument board, still keeping it fully to the left. The A.S.I. reading should be noted. If the column has been pushed forward in time the autogiro will not swing far. Shortly after the swing ceases the A.S.I. needle will start to creep up the scale. This must be instantly checked by pulling the column hard back and to the right to check the tendency to swing left consequent on the backward movement of the column. The A.S.I. needle will then creep down towards the critical speed, and the cycle of operations must be repeated. With practice it is possible to anticipate the movements of the autogiro with sufficient accuracy to keep the A.S.I. needle close to the critical speed. By this method angles of descent approaching the vertical are attainable, though the direction of the autogiro is not constant. It appears that if the A.S.I. needle is held 1 m.p.h. above the critical speed and never allowed to go below it the direction can be kept constant, though with some loss in steepness of descent.

11.5. *The take-off.*—The take-off is accomplished in three stages :—

(*a*) Starting the rotor with the autogiro stationary.

(*b*) Accelerating the whole aircraft with the rotor disc at minimum incidence (stick forward).

(*c*) Establishing autorotation by increasing disc incidence, and thus accelerating blades to the speed of rotation necessary to lift autogiro off ground.

During stage (*a*) the wheel brakes are on, and the engine is used to accelerate the rotor. At the end of stage (*a*) the wheel brakes and the rotor clutch are released simultaneously by the operation of one lever. Stage (*b*) then begins. The rotor decelerates during this stage, since there is insufficient air flow through the disc to maintain autorotation. The necessary flow is built up by allowing the whole aircraft to accelerate. To obtain the best acceleration the control column is held forward to keep the rotor drag at its lowest possible amount. Having, at the end of stage (*b*), attained sufficient air speed to establish autorotation, stage (*c*) is entered by pulling the control column slowly, but firmly, back to its full extent. During stage (*c*) autorotation sets in and the rotor accelerates. When the rotor revolutions reach a certain value (a function of the loading) the autogiro lifts off the ground.

It will be obvious from the foregoing that the length of the ground run, and the time occupied in getting off depend on the wind speed, the rotor revolutions at the end of stage (*a*), and the load.

11.6. *Landing.*—Landing from steep descent with the engine on is merely a special case of slow flying, which has been dealt with in paragraph 4 (*b*). (See also note on checking of drift, below.)

Landing with the engine off necessitates two things :—

(*a*) Having a minimum gliding speed of 40 m.p.h. just before flattening out.

(*b*) Having no drift when touching down.

As far as (*a*) is concerned, the method of approach is of no consequence so long as the final condition is satisfied. With regard to (*b*), for obvious reasons only the smallest amount of drift is permissible on touching down. The limits in this connection are so fine that it is not possible to tell until quite near the ground whether the drift has been reduced to a safe amount. If not, due to the sluggishness of the control, there is then hardly time to bank the autogiro sufficiently to make the correction and level up again before touching down. If the first attempt to correct drift has been unsuccessful, it becomes necessary to keep the autogiro in the air by using the engine until the drift is small enough to allow a safe touch down. The result is that the final landing is probably made a good many yards from the spot first chosen. On days when there is a light wind varying in direction from point to point

on the aerodrome, or a gusty wind, this inability to correct for drift at the last moment (or to steer round an obstacle when slow flying) is a serious disadvantage of a control which, within the normal speed range, is extremely simple and almost foolproof.

11.7. *View downwards and ahead.*—A bad point in design, which has its effect in slow flying and steep descent, is the shape of the fuselage. In plan view the side of the fuselage extends too far beyond the edge of the entrance to the cockpit. This obstructs the view downwards at all times, and ahead when the nose is high (as in slow flying). There are several methods of remedying this, of which a wide sliding panel in the side of the fuselage is probably the best, since it has the added advantage of making an emergency exit from the cockpit easier.

11.8. *Lateral bias control.*—The lateral bias could be improved by operating it by the single stroke of a lever (as for the fore and aft bias). Even if the present from of operation is retained, it should have an indicator showing the position of the control.

11.9. *The control column.*—If it became necessary to make a parachute descent from a direct control autogiro, the present form of hanging control column would greatly hinder the pilot from getting out of the cockpit. If the rotor were damaged, the hanging column would probably thrash about the cockpit in so violent a fashion as to make exit without injury impossible. The possibility of breaking the hanging column near the rotor head and allowing it to hinge in the fore and aft direction, and arranging some form of bolt to restrain hinge movement normally but capable of withdrawal in an emergency, might be considered. This, coupled with the sliding panel suggested in §11.7, would make it much easier to get out of an autogiro if forced to do so (naturally this only applies to autogiros whose occupants wear parachutes).

11.10. *Rudder for low speeds.*—A possible improvement in the yawing control at low speeds might be obtained in the following manner. The present adjustable portion of the fin might be increased in size until it assumes the proportions of a small rudder. It could then be connected so as to operate by the lateral movement of the control column. A linkage could be incorporated so that by setting a small lever in the cockpit in one position the rudder would remain central all the time, and by setting it in another the rudder would follow the movements of the column. The direct control would then be unaltered for normal flying, and have the aid of a rudder for slow flying.

11.11. *Range of fore and aft control.*—It would be advantageous if some means of increasing the power of the control to get the autogiro out of a dive could be found. This might be done by fitting an elevator and connecting it to the fore and aft bias control. The simplicity of the direct control should make the autogiro an easy craft to fly in clouds and conditions of bad visibility, but the possibility of getting into a dangerous dive makes blind flying definitely unsafe.

12. APPENDIX II

Measurement of parasitic drag of fuselage

12.1. *Introduction.*—In connection with the analysis of performance, a 1/8th scale model of the fuselage was tested in the National Physical Laboratory 7-ft. No. 3 tunnel. The drag was measured later in the Compressed Air Tunnel over a range of Reynolds numbers extending from the above atmospheric tunnel tests to full scale top speed.

At the same time the opportunity was taken of checking an estimate used in R. & M. 1727[11] of the lift curve of the tail plane in the absence of down wash from the rotor. (It should be remarked that the tail plane, of symmetrical section, was set at 0° to the body datum. On the full scale aircraft the tail plane, which has upturned tips, is cambered; but one half is inverted in order to take the airscrew torque, the corresponding mean angle being +2°.)

12.2. *Experimental details.*—The measurements were made in the National Physical Laboratory 7-ft. No. 3 tunnel, the model (Fig. 16), correct way up, being suspended from two roof balances. The forward (lift) balance was attached directly by wires to the sides of the fuselage near the position corresponding to the C.G. in the full scale aircraft, and the spindle of a drag and vertical force balance to a sting continuing the tail. From the three readings at each angle and wind speed the lift, drag and pitching moment were deduced in the usual way.

With the model complete as above, measurements were made first at 60 ft./sec. over an incidence range —4° to +26° and at 0° for a wind speed range 40–90 ft./sec. The tail plane was then removed, leaving the fuselage sides flush at the tail, and both sets of readings were repeated. Since a considerable scale effect was evident, the further measurements when parts of the model were successively removed were mostly made for the complete speed range 40–90 ft./sec. at zero incidence. These further removals were (after the tail plane) (1) rotor hub, (2) engine and exhaust ring, (3) complete undercarriage, (4) windscreens, (5) rotor pylon and tail wheel; leaving finally the body stripped of all but the tail fins and fixed rudder, which were not conveniently detachable.

Tables 12 and 13 of results are given at the end of the report, where also they have been reduced to a common basis of full scale at 100 ft./sec.

12.3. *Scale effect.*—The reduced results are plotted for convenience on a doubly logarithmic base in Fig. 39 and it is at once evident that there is a considerable scale effect on those parts of the drag due to the undercarriage and to the pylon carrying the rotor. This is in accordance with the known large scale effect occurring in the case of thick struts.[18] In extrapolating to the full scale value this has been taken into account, and the approximate figure of 90 lb. at 100 ft./sec. is arrived at for the parasitic drag of the whole aircraft at zero incidence, to which the various components contribute as follows: —

Undercarriage and its wheels	29 lb.
Engine and exhaust ring	17 ,,
Pylon	10 ,,
Fuselage, with vertical fins	11 ,,
Rotor hub	10 ,,
Tail plane	7 ,,
Windscreens	4½ ,,
Tail wheel	1½ ,,
Total	90 lb.

As some sort of check on the undercarriage drag, which is the largest item and also the one to which the scale effect applies most, a rough estimate was made on the basis of R. & M. 579[18] of the drag to be expected at model and full scale, all figures as usual being reduced to full scale at 100 ft./sec.

	⅛ model at 60 ft./sec.	*Full scale.*
2 Wheels	6·5 lb.	5·3 lb.
Struts	14·0 ,,	5·6 ,,
2 Wheel- and 6 Body-joints	10·0 ,,	10·0 ,,
20 per cent. allowance for interference	6·1 ,,	4·2 ,,
Totals	36·6 lb.	25·1 lb.

Since the measured value is by subtraction 46·5 lb. at model scale and 60 ft./sec., we should increase the full scale figure in proportion, and obtain 32 lb., comparing with the extrapolated value of 29 lb. of Fig. 38.

12.4. *Incidence.*—In Fig. 40 the lift and drag variations with incidence are plotted for the two cases tail plane present and removed.

By subtraction the tail plane characteristics are easily found. Its lift curve has a slope of 0·0863 lb. per degree incidence at 60 ft./sec. and model scale, which gives for the full scale machine $1 \cdot 53 \times V^2S$ lb. per radian at 100 ft./sec. This is in good agreement with the value 1·5 for the coefficient assumed in reference 11 in calculating the pitching equilibrium of the aircraft.

It will be observed that a certain amount of negative lift is developed on the body without tail plane. At full scale this appears to be of the order — 23 lb. at 100 ft./sec., and zero incidence and does not disappear till an incidence of 15° is reached. It may be of interest to note that by setting the tail plane at +2°, as it is in practice on full scale, this lift is just cancelled out.

12.5. *Measurement of drag in the Compressed Air Tunnel.*—A recent determination has been made in the Compressed Air Tunnel of the drag of the same model, at a number of velocities and pressures corresponding to a range of Reynolds number extending from the above 7-ft. tunnel tests to full scale top speed.

The measurements made were of drag on the complete model (without rotor blades) at zero incidence, which enables an estimate to be made of the scale effect. The results are tabulated in Table 15 and plotted in Fig. 41, being there reduced to lb. at full scale and 100 ft./sec., and compared with the values found in the atmospheric tunnel.

It will be seen that a value of 82 lb., somewhat lower than the previous estimate, is obtained at the full scale Reynolds number. It may however be permissible to consider the figure of 90 lb. used in the calculations as including an allowance for imperfections of the surface on the full scale aircraft.

It is interesting to note that on the log-log basis, the results are grouped along a nearly straight line, as had been assumed in the extrapolation from the atmospheric tunnel results to full scale.

The authors wish to acknowledge their indebtedness to the staff of the Compressed Air Tunnel for making these measurements.

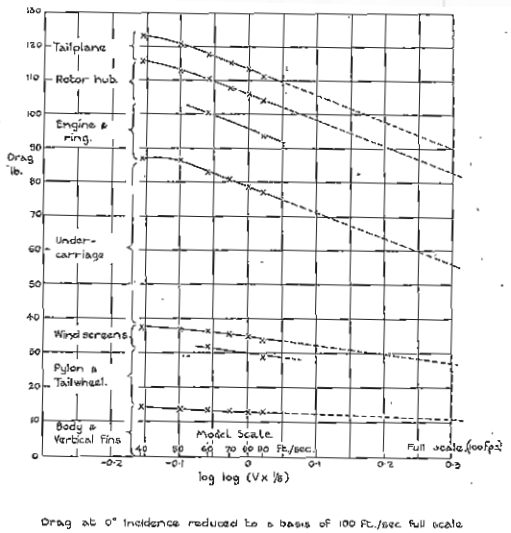

FIG. 39.—Parasitic drag of C.30 Autogiro as measured on a ⅛ scale model in the 7-ft. No. 3 wind tunnel.

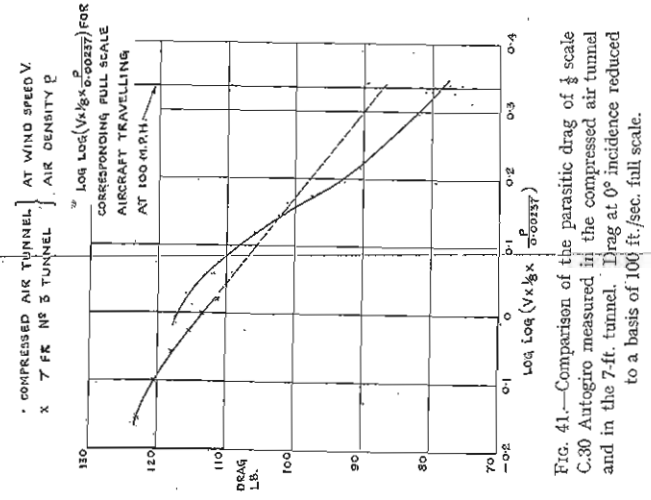

FIG. 41.—Comparison of the parasitic drag of ⅛ scale C.30 Autogiro measured in the compressed air tunnel and in the 7-ft. tunnel. Drag at 0° incidence reduced to a basis of 100 ft./sec. full scale.

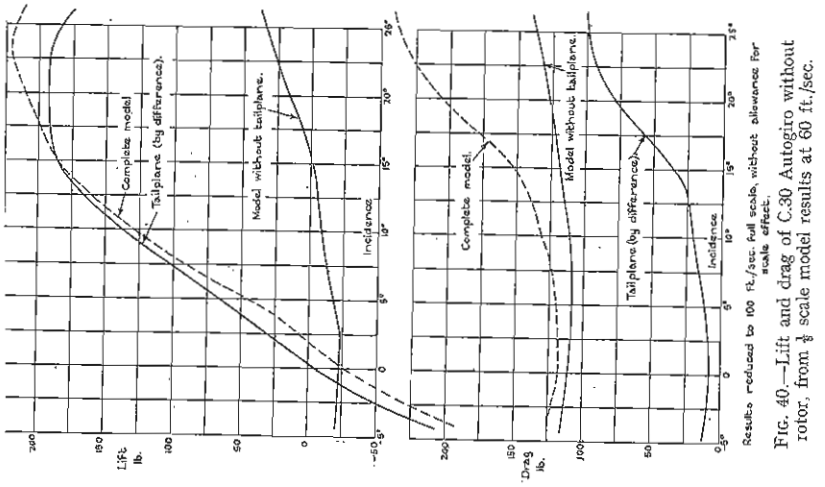

FIG. 40.—Lift and drag of C.30 Autogiro without rotor, from ⅛ scale model results at 60 ft./sec.

13. APPENDIX III

Modifications to rotor theory to correct for various approximations

13.1. *Tip loss.*—Owing chiefly to tapering of the section the aerodynamic forces on the blade near the tip are not such as have been so far assumed (in R. & M. 1127[4] and 1727[11]), *i.e.*, arising from a uniform blade and with no induced end effects on the flow. An allowance has therefore been made firstly on the assumption that the lift *coefficient* is constant whatever the chord, while the profile drag is not reduced by the presence of taper. With the plan form of the C.30 blades this is equivalent to a complete loss of lift on the tip 0·25 chord of blade. Secondly, for an airscrew of the shape and dimensions of the autogiro rotor moving *axially* with velocity V sin i, a calculation on the basis of R. & M. 1674[19] determines a reduction of lift coefficient at the extreme tip equivalent to a loss of lift on a further 0·065 chord of blade. However except near $\mu = 0$ the flow is far from axial and this effect might even be much smaller. It has accordingly been neglected in the calculations for $\mu \gtrsim 0$.

To take account of this loss Wheatley's method[9] has been followed, the modified general rotor equations being derived by integrating along the blade to a point short of the tip, say to a radius BR where R — BR (= 0·25 chord in our case) is the equivalent length of blade over which complete loss occurs. The integration is however to the tip for terms involving the profile drag (coefficient δ). The new equations are (*cf.* (11)–(15) of R. & M. 1727) :—

Zero thrust moment

$$-\frac{1}{\gamma}a_0 + \frac{1}{3}\lambda B^3 + \frac{1}{4}(B^4 + \mu^2 B^2)\,\theta_0' - \frac{1}{3}\mu\theta_1 B^3 - \frac{1}{\gamma}C' = 0$$

$$-\frac{1}{3}\mu a_0 B^3 + \frac{1}{4}\left(B^4 + \frac{1}{2}\mu^2 B^2\right)b_1 = 0$$

$$\frac{1}{2}\mu\lambda B^2 - \frac{1}{4}\left(B^4 - \frac{1}{2}\mu^2 B^2\right)a_1 + \frac{2}{3}\mu\theta_0' B^3 - \frac{1}{4}\left(B^4 + \frac{3}{2}\mu^2 B^2\right)\theta_1 = 0.$$

Zero torque

$$\lambda^2 B^2 + \mu\lambda a_1 B^2 + \frac{2}{3}\lambda\theta_0' B^3 - \frac{1}{2}\mu\lambda\theta_1 B^2 + \frac{1}{2}\mu^2 a_0^2 B^2 - \frac{2}{3}\mu a_0 b_1 B^3$$

$$+ \frac{1}{4}\left(B^4 + \frac{3}{2}\mu^2 B^2\right)a_1^2 + \frac{1}{4}\left(B^4 - \frac{1}{2}\mu^2 B^2\right)a_1\theta_1 + \frac{1}{4}\left(B^4 + \frac{1}{2}\mu^2 B^2\right)b_1^2$$

$$-\frac{\delta}{2a}(1+\mu^2) = -\frac{4}{a}q = 0.$$

Thrust

$$t = \frac{1}{2}a\left\{\frac{1}{2}\lambda B^2 + \frac{1}{3}(B^3 + \frac{3}{2}\mu^2 B)\,\theta_0' - \frac{1}{2}\mu B^2\theta_1\right\}.$$

As will be seen from Table 14 summarising the corrections, tip loss reduces the thrust by a fairly constant amount of some 70–80 lb. but has otherwise little effect.

13.2. *0.7R approximation.*—A few further values of μ were worked out by the method fully described in Appendix IV of R. & M. 1727,[11] which takes account in the general rotor equations of the variation of pitch along the blade as well as around the circle.

Here the correction is hardly appreciable, except on thrust at the higher values of μ, where it is of the order + 70 lb. at top speed.

13.3. *Radial flow.*—Up till now it has been assumed that the only aerodynamic forces acting on a section of blade are those appropriate to the components of relative air velocity in the plane perpendicular to the blade axis. Glauert, in an appendix to R. & M. 1111,[2] has discussed on an energy basis the effect of allowing for the radial component of drag, obtaining a direct correction on the lift/drag ratio. A different method has been adopted here in order to derive the separate corrections on incidence, thrust, longitudinal force, etc., but the results have been checked against Glauert's formula.

To the first order the radial component of velocity is $\mu R\Omega \cos\psi$ (notation of R. & M. 1727,[11] Appendix I) and the circumferential component $r\Omega + \mu R\Omega \sin\psi$, at radius r. Let $\eta = \tan^{-1}\left\{\mu R\Omega \cos\psi/(r\Omega + \mu R\Omega \sin\psi)\right\}$ be the angle between the resultant of these and the perpendicular to the blade.

Then the drag on an element dr of blade is

$$\frac{1}{2}c\varrho\delta\left\{(r\Omega + \mu R\Omega \sin\psi)^2 + \mu^2R^2\Omega^2\cos^2\psi\right\}dr$$

$$= \frac{1}{2}c\varrho\delta\Omega^2R^3\,(x^2 + 2x\,\mu\sin\psi + \mu^2)\,dx$$

acting along the resultant.

Hence the profile drag term in the equation of zero torque (equation (14) of R. & M. 1727) is :—

$$\frac{-4}{Nc\varrho R^4\Omega^2a}\times\frac{N}{2\pi}\int_0^{2\pi}d\psi\int_0^1\frac{1}{2}c\varrho\delta\Omega^2R^3\,(x^2 + 2x\mu\sin\psi + \mu^2)\cos\eta\,r\,dx$$

$$= \frac{-\delta}{a\pi}\int_0^{2\pi}d\psi\int_0^1 x\,(x + \mu\sin\psi)\,(x^2 + 2x\mu\sin\psi + \mu^2)^{\frac{1}{2}}\,dx$$

and in the expression for the longitudinal force (equation (16) of R. & M. 1727) :

$$\frac{1}{Nc\varrho R^3\Omega^2}\times\frac{N}{2\pi}\int_0^{2\pi}d\psi\int_0^1\frac{1}{2}c\varrho\delta\Omega^2R^3(x^2 + 2x\mu\sin\psi + \mu^2)\sin(\eta + \psi)dx$$

$$= \frac{\delta}{4\pi}\int_0^{2\pi}d\psi\int_0^1(x\sin\psi + \mu)\,(x^2 + 2x\,\mu\sin\psi + \mu^2)^{\frac{1}{2}}\,dx\ .$$

In default of simple integrals of these expressions Glauert's method[2] of obtaining approximations by evaluating the inner integrals at the points $\psi = 0$, 90°, 180° and 270° and averaging has been adopted. The respective expressions then become :—

$$-\frac{\delta}{2a}\left\{\frac{1}{2}(1 + \frac{1}{2}\mu^2)\sqrt{1 + \mu^2} - \frac{1}{4}\mu^4\log\left(\frac{1}{\mu} + \sqrt{1 + \frac{1}{\mu^2}}\right) + \frac{1}{2} + \mu^2\right\}$$

and

$$\frac{\delta}{8}\left\{\mu\sqrt{1 + \mu^2} + \mu^3\log\left(\frac{1}{\mu} + \sqrt{1 + \frac{1}{\mu^2}}\right) + 2\mu\right\}$$

instead of $-\frac{\delta}{2a}(1 + \mu^2)$ and $\frac{1}{4}\mu\delta$ when radial flow is ignored.

When the correction in the zero torque equation is made, slightly increased values of the rotor characteristics (velocity through the disc $\lambda R\Omega$, flapping angles a_0, a_1, b_1 and twist θ_0) are obtained, with consequent changes in thrust T and incidence i. The longitudinal force H is also increased indirectly by a small amount in addition to that given by the expression found above. As may be seen from Table 14 this alteration of H is the most important consequence of taking radial flow into account, introducing at top speed an addition of 20 lb. to the drag of the aircraft.

13.4. *Rotor speed.*—In the calculations of R. & M. 1727 the procedure was to determine separately for each value of μ the steady state of working of the rotor, using, apart from the physical constants of the blades, no experimental data except the angular velocity of the rotor as measured in gliding tests. Since this rotor speed has been found to be somewhat uncertain it has been thought advisable to apply a further correction at each speed, of such magnitude that the final thrust is equal to that necessary to take the known weight of the aircraft. (In the case of level flight under power this lift includes an allowance for the vertical component of airscrew thrust as well as for tail plane and body lift.)

Although the major effect of changing the rotor speed is, as might be expected, to vary the thrust approximately according to the square of the ratio of the speeds, a more complete investigation has been made to find the effects on the other characteristics. This was done simply by differentiating the pitch and general rotor equations ((9)–(14) of R. & M. 1727) for the small changes $\Delta\lambda$, Δa_0, Δa_1, Δb_1, $\Delta\theta_0$, $\Delta\theta_1$ due to a small change $\Delta\Omega$, and then solving for these at each μ using the previous numerical values of Ω, λ, a_0, etc. By a similar differentiation of equations (15), (17) and (19) the corresponding changes in the coefficients t, i and h, and finally T and H, were obtained.

The results are shown in Table 14 being expressed in terms of a 1 per cent. increase of rotor speed. They have also been used there to make the final correction discussed above and hence to give the correct lift in the two cases of steady horizontal flight under power and steady gliding.

REFERENCES

No.	*Author.*	*Title, etc.*
1	H. E. Wimperis	The rotating wing in aircraft. R. & M. 1108. August, 1926.
2	H. Glauert	A general theory of the autogiro. R. & M. 1111. November, 1926.
3	L. E. Caygill and A. E. Woodward Nutt.	Wind tunnel and dropping tests of autogiro models. R. & M. 1116. November, 1926.
4	C. N. H. Lock	Further developments of autogiro theory. R. & M. 1127. March, 1927.
5	C. N. H. Lock and H. C. H. Townend.	Wind tunnel experiments on a model autogiro at small angles of incidence. R. & M. 1154. March, 1928.
6	H. Glauert and C. N. H. Lock ..	A summary of the experimental and theoretical investigations of the characteristics of an autogiro. R. & M. 1162. April, 1928.
7	John B. Wheatley..	Lift and drag characteristics of gliding performance of an autogiro as determined in flight. N.A.C.A. Report No. 434. 1932.
8	John B. Wheatley..	Wing pressure distribution and rotor-blade motion of an autogiro as determined in flight. N.A.C.A. Report No. 475. 1934.
9	John B. Wheatley..	An aerodynamic analysis of the autogiro rotor with a comparison between calculated and experimental results. N.A.C.A. Report No. 487. 1934.
0	R. S. Capon	The representation of aircraft performance tests, using non-dimensional variables, with special reference to the prediction of the effects of change of loading on performance. R. & M. 984. November, 1925.
1	J. A. Beavan and C. N. H. Lock	The effect of blade twist on the characteristics of the C.30 autogiro. R. & M. 1727. April, 1936.
2	C. N. H. Lock and H. Bateman ..	An analysis of tests in the N.A.C.A. propeller research tunnel. A.R.C. Report 2765. (Ae. Tech. 1174) unpublished. December, 1936. *See also* R. & M. 1849—"A graphical method of calculating the performance of an airscrew," and Handbook of Aeronautics.
3	John B. Wheatley and Manley J. Hood.	Full scale wind tunnel tests of a PCA-2 autogiro rotor N.A.C.A. Report No. 515. 1935.
4	A. G. Pugsley and T. G. Husbands	Some photographic results on the flexure of the rotor blades of a gyroplane. R.A.E. Report No. A.D.3064. (2075—Ae. Tech. 994) unpublished.
5	R. A. Frazer, W. P. Jones and Miss S. W. Skan.	Approximations to functions and to the solutions of linear differential equations. R. & M. 1799. March, 1937.
6	Scarborough	Numerical mathematical analysis. Chapter XVII.
7	John B. Wheatley	A study of autogiro rotor blade oscillations in the plane of the rotor disc. N.A.C.A. Tech. Note 581. September, 1936.
8	The Aerodynamic Staff of the R.A.E.	The resistance of aeroplane undercarriages of two types, and of wheels. R. & M. 579. February, 1919.
9	C. N. H. Lock and D. Yeatman ..	Tables for use in an improved method of airscrew strip theory calculation. R. & M. 1674. October, 1934.

TABLE 10

Particulars of autogiro C.30

Gross weight as flown	1,900 lb.
Diameter of rotor	37 ft.
Number of blades	3.
Chord of blades	11 in.
Blade section	Göttingen 606.
Solidity	0·0472.
Blade angle	2° 40′ (approx.)
Inclination of rotor axis to plane perpendicular to fuselage datum.*	2½° forward, 7½° back.
Lateral inclination of rotor axis to vertical plane parallel to fuselage datum*	5° to right, 4° to left.
Position of C.G.	6·0 in. aft of intersection of front pylon struts and top longerons.
Area of tail plane	15·6 sq. ft.
Total fin area	16·3 sq. ft.
Tail incidence	+ 2°.
Ground angle	10°.
Engine	Civet I.
Max. power	152 H.P. at 2,420 r.p.m (log book).
Airscrew	Fairey Reed, two blader Drg. No. 95193A/X2.
Pitch (measured)	4·33 ft.
Diameter (measured)	7·0 ft.

* The fuselage datum is parallel to the top longerons.

TABLE 11

Results from glides

V_E m.p.h.	$i - \gamma$ (deg.)	γ (deg.)	C_L	C_D	μ
31·2	− 1·1	17·25	0·654	0·204	0·112
78·8	− 8·1	12·55	0·103	0·023	0·272
22·9	+ 0·4	28·55	1·092	0·594	0·076
57·6	− 5·4	11·1	0·192	0·038	0·211
49·2	− 3·9	11·8	0·260	0·054	0·182
69·4	− 7·4	11·7	0·136	0·028	0·241
57·7	− 6·1	11·4	0·195	0·040	0·210
48·9	− 4·8	12·0	0·270	0·058	0·180
73·6	—	12·2	0·120	0·026	—
28·2	− 0·3	19·65	0·800	0·286	0·099
33·6	− 1·65	16·15	0·570	0·165	0·121
36·2	− 1·8	15·15	0·491	0·133	0·131
22·4	− 0·25	35·6	1·066	0·764	0·069
25·2	− 0·2	23·2	0·948	0·406	0·087
40·4	− 1·7	12·45	0·398	0·088	0·146
23·5	− 0·15	25·3	1·088	0·514	0·079
59·9	− 5·55	11·2	0·180	0·036	0·217
55·3	− 4·75	10·95	0·210	0·041	0·201
22·5	+ 0·4	29·7	1·108	0·632	0·074
89·0	− 9·45	13·35	0·083	0·020	0·294
40·8	− 1·75	12·85	0·392	0·090	0·147
41·1	− 2·2	12·20	0·380	0·082	0·150
24·4	+ 0·7	24·00	1·004	0·448	0·065
26·3	− 0·7	21·55	0·894	0·352	0·092
25·2	− 0·3	23·5	0·954	0·416	0·086
24·5	− 0·2	23·75	1·000	0·440	0·084
23·5	+ 0·5	26·15	1·060	0·520	0·079
52·5	− 4·95	11·1	0·232	0·046	0·191
54·4	− 4·8	11·25	0·214	0·042	0·198
40·3	− 2·4	13·2	0·406	0·095	0·145
38·2	− 1·75	13·35	0·448	0·107	0·138
50·8	− 3·3	10·6	0·254	0·048	0·183
23·3	+ 0·85	26·3	1·092	0·542	0·078
23·8	+ 0·9	26·25	1·044	0·507	0·078
24·6	+ 0·2	23·25	1·012	0·434	0·085
23·1	+ 0·05	27·5	1·092	0·567	0·077
22·7	+ 0·85	38·7	1·032	0·826	0·064
23·8	+ 0·2	27·0	1·066	0·543	0·079
22·5	+ 0·35	33·5	1·112	0·734	0·070
21·8	− 0·75	63·2	0·636	1·258	0·037
21·9	+ 1·4	60·3	0·684	1·196	—
92·8	− 9·0	13·6	0·074	0·018	0·305
96·3	−11·7	15·6	0·068	0·019	0·315
90·5	− 9·65	13·2	0·077	0·018	0·307
22·1	+ 3·6	68·45	0·484	1·228	0·025
22·1	+ 1·05	45·6	0·916	0·934	0·058

TABLE 12

Tests on a 1/8 scale model of the C.30 Autogiro (without rotor) in 7-ft. No. 3 Wind Tunnel

Complete Model tested at 60 ft./sec. (corrected for spindle and wires drag)

Incidence.	Lift. (lb.)	Drag. (lb.)	Pitching Moment. (lb.-ft.)	Equivalent full scale at 100 ft./sec. Lift. (lb.)	Drag. (lb.)	Pitching Moment. (lb.-ft.)
− 4°	−0·603	0·7039	0·555	−107·1	125·1	790
− 2°	−0·347	0·6888	0·250	− 61·6	122·3	356
0	−0·149	0·6676	0·041	− 26·5	118·8	58
2°	+0·001	0·6628	−0·141	+ 0·2	117·9	− 200
4°	0·151	0·6705	−0·287	26·8	119·2	− 409
6°	0·364	0·6839	−0·480	64·7	121·5	− 683
8°	0·561	0·7005	−0·672	99·8	124·6	− 956
10°	0·727	0·7401	−0·850	129·3	131·5	−1210
14°	0·999	0·8204	−1·063	177·6	145·9	−1513
18°	1·130	1·0372	−1·210	200·8	184·2	−1721
22°	1·225	1·245	−1·280	217·8	221·4	−1821
26°	1·198	1·350	−1·130	212·8	240·0	−1608
			Tailplane removed. 60 ft./sec.			
− 4°	−0·118	0·6459	−0·045	− 21·0	115·0	− 64
0	−0·125	0·6241	+0·027	− 22·2	110·9	+ 38
2°	−0·133	0·6155	0·038	− 23·6	109·4	54
6°	−0·088	0·6105	0·094	− 15·6	108·6	134
10°	−0·050	0·6241	0·127	− 8·9	110·9	181
14°	−0·017	0·6609	0·198	− 3·2	117·6	282
18°	0·048	0·6942	0·239	+ 8·5	123·2	340
22°	0·137	0·7317	0·266	24·4	130·1	378
26°	0·211	0·7865	0·312	37·5	139·9	444

TABLE 13

Model tested at 0° incidence over a range of wind speed

	Wind speed. (ft./sec.)	Lift. (lb.)	Drag. (lb.)	Pitching moment. (lb.-ft.)	Equivalent full scale at 100 ft./sec. Lift. (lb.)	Drag. (lb.)	Pitching moment. (lb.-ft.)
Complete model	40	−0·049	0·3074	0·021	−19·6	128·0	67
	50	−0·096	0·4708	0·031	−24·6	120·6	64
	60	−0·144	0·6625	0·031	−25·6	117·9	44
	70	−0·230	0·8824	0·062	−30·0	115·2	65
	80	−0·333	1·1354	0·093	−33·3	113·5	74
	90	−0·441	1·4071	0·155	−34·8	111·1	97
Tailplane removed	40	−0·038	0·2892	0·010	−15·2	115·7	32
	50	−0·071	0·4395	0·010	−18·2	112·5	29
	60	−0·120	0·6211	0·016	−21·3	110·4	23
	70	−0·191	0·8227	0·037	−25·0	107·4	39
	80	−0·263	1·0606	0·016	−26·3	106·1	13
	90	−0·355	1·3132	0·048	−28·0	103·9	30
Rotor hub also removed	60	−0·099	0·5641	−0·031	−17·6	100·2	− 44
	90	−0·325	1·1827	−0·062	−25·7	93·5	− 39
Engine and exhaust ring also removed.	40	−0·038	0·2168	−0·010	−15·2	86·7	− 32
	50	−0·067	0·3360	−0·021	−17·2	86·1	− 43
	60	−0·114	0·4663	−0·021	−20·3	83·0	− 30
	70	−0·182	0·6158	−0·031	−23·8	80·5	− 32
	80	−0·263	0·7882	−0·041	−26·3	78·8	− 33
	90	−0·357	0·9746	−0·052	−28·2	77·0	− 33
Undercarriage also removed	40	−0·020	0·0946	0·064	− 8·0	37·8	203
	50	−0·023	0·1439	0·081	− 5·9	36·8	166
	60	−0·023	0·2043	0·091	− 4·1	36·4	129
	70	−0·036	0·2725	0·122	− 4·7	35·6	127
	80	−0·056	0·3486	0·163	− 5·6	34·9	130
	90	−0·076	0·4234	0·205	− 6·0	33·5	130
Windscreens also removed	60		0·1794			31·9	
	90		0·3632			28·7	
Rotor pylon and tailwheel also removed (leaving only body and fins).	40	−0·009	0·0364	0·027	− 3·6	14·6	86
	50		0·0540			13·8	
	60		0·0758			13·5	
	70		0·0997	0·072		13·1	75
	80		0·1285			12·9	
	90	−0·058	0·1630	0·130	− 4·6	12·9	82

TABLE 14

Calculation of performance—Corrections for various factors (see *Appendix III*)

Rotor Characteristics.	$\mu = 0$			$\mu = 0·1$			$\mu = 0·15$		
	i	T	H	*i*	T	H	*i*	T	H
Uncorrected figures for δ=0·014 as in R. & M.1727.	90°	2128	0	21·65°	1980	46·5	10·97°	1955	67·3
Correction for tip loss	0	−83	0	0·02°	−78	−2·0	0·03°	−75	− 2·4
Correction for 0.7R approximation.	0	11	0	0·05°	6	−1·5	0·08°	9	− 2·5
Correction for radial flow	0	0	0	0·05°	3	4·0	0·06°	5	6·2
Addition for change of δ from 0·014 to 0·012	0	−67	0	−1·35°	−66	−3·5	−0·86°	−69	− 5·3
Hence, corrected values $\delta = 0·014$	90°	2056	0	21·77°	1911	47·0	11·14°	1894	68·6
$\delta = 0·012$	90°	1989	0	20·42°	1845	43·5	10·28°	1825	63·3
Correction for 1 per cent. increase in rotor speed.	0	41	0	0·01°	38	0·5	0·02°	36	0·6
Hence, final values to give correct lift *in level flight* $\delta = 0·014$	90°	(1900)	0	21·77°	1903	46·9	11·16°	1921	69·1
$\delta = 0·012$	90°	(1900)	0	20·44°	1903	44·3	10·33°	1921	64·9
And, final values to give correct lift *in gliding* $\delta = 0·014$	90°	(1900)	0	21·76°	1887	46·7	11·14°	1898	68·7
$\delta = 0·012$	90°	(1900)	0	20·43°	1887	44·1	10·32°	1898	64·5

	$\mu = 0·2$			$\mu = 0·25$			$\mu = 0·3$		
	i	T	H	*i*	T	H	*i*	T	H
Uncorrected, $\delta = 0·014$	6·57°	1937	82·8	4·37°	1948	95·0	3·32°	1955	99·8
Tip loss	0·05°	−73	−2·4	0·07°	−70	−2·2	0·10°	−67	− 2·0
0.7R approximation	0·12°	15	−3·7	0·15°	35	−5·3	0·19°	72	− 7·0
Radial flow	0·08°	8	8·8	0·09°	12	12·2	0·10°	19	17·0
Change of δ to 0·012	−0·61°	−73	−7·5	−0·46°	−79	−9·6	−0·35°	−85	−11·8
Corrected, $\delta = 0·014$	6·82°	1887	85·5	4·68°	1925	99·7	3·71°	1979	107·8
$\delta = 0·012$	6·21°	1814	78·0	4·22°	1846	90·1	3·36°	1894	96·0
1 per cent. increase in rotor speed.	0·04°	35	0·5	0·05°	34	0·3	0·07°	33	− 0·2
Final values for *level flight* $\delta = 0·014$	6·88°	1937	86·2	4·71°	1944	99·9	3·63°	1941	108·0
$\delta = 0·012$	6·35°	1937	79·8	4·36°	1944	91·0	3·46°	1941	95·7
Final values for *gliding* $\delta = 0·014$	6·83°	1897	85·6	4·63°	1889	99·4	3·50°	1880	108·4
$\delta = 0·012$	6·30°	1897	79·2	4·28°	1889	90·5	3·33°	1880	96·1

TABLE 15

Drag of 1/8 scale C.30 autogiro model in the compressed air tunnel

Density ϱ.	Velocity V.	Log log $(V \times \frac{1}{8} \times \varrho/0{\cdot}00237)$	Drag coefficient $D/\frac{1}{2}\varrho V^2$.	Equivalent drag at full scale 100 ft./sec.
	ft./sec.			lb.
0·00234	79·3	−0·004	0·1544	117·2
0·00355	50·0	−0·013	0·1542	117·1
	62·4	0·028	0·1527	115·8
	74·9	0·059	0·1472	111·8
	84·8	0·080	0·1476	112·0
0·00682	36·0	0·046	0·1493	113·3
	43·2	0·076	0·1462	111·0
	50·4	0·100	0·1406	106·7
	57·6	0·119	0·1394	105·9
	68·4	0·143	0·1348	102·2
	79·6	0·163	0·1332	101·1
0·00979	48·1	0·145	0·1341	101·9
	60·1	0·173	0·1283	97·5
	72·2	0·196	0·1231*	93·5
			0·1223*	92·9
	87·0	0·218	0·1189	90·3
0·01765	40·3	0·197	0·1043	79·2
	51·5	0·226	0·1186	90·0
	64·8	0·251	0·1135	86·2
	80·7	0·273	0·1118	84·9
0·02925	49·5	0·275	0·1106*	83·9
			0·1167*	88·5
	62·7	0·298	0·1080	82·0
	76·7	0·317	0·1077	81·7
	87·4	0·328	0·1012	76·9
0·0401	57·2	0·319	0·1046*	79·4
			0·1067*	81·0
	64·7	0·330	0·1069	81·1
	72·3	0·339	0·1019*	77·3
			0·0998*	75·7
			0·1051*	79·8
	80·5	0·348	0·1119	84·9

* Multiple readings.

(46827) Wt. 2/3766 500 2/40. Hw. G.377/1

SYSTEM OF AXES

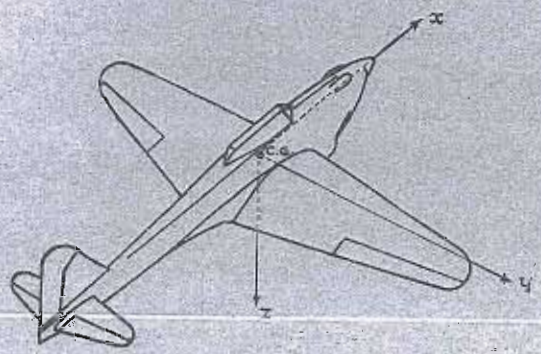

Axes	Symbol Designation Positive direction	x longitudinal forward	y lateral starboard	z normal downward
Force	Symbol	X	Y	Z
Moment	Symbol Designation	L rolling	M pitching	N yawing
Angle of Rotation	Symbol	ϕ	θ	ψ
Velocity	Linear	u	v	w
	Angular	p	q	r
Moment of Inertia		A	B	C

Components of linear velocity and force are positive in the positive direction of the corresponding axis.

Components of angular velocity and moment are positive in the cyclic order y to z about the axis of x, z to x about the axis of y, and x to y about the axis of z.

The angular movement of a control surface (elevator or rudder) is governed by the same convention, the elevator angle being positive downwards and the rudder angle positive to port. The aileron angle is positive when the starboard aileron is down and the port aileron is up. A positive control angle normally gives rise to a negative moment about the corresponding axis.

The symbols for the control angles are:—

ξ aileron angle
η elevator angle
η_T tail setting angle
ζ rudder angle